JOURNAL OF GEOPHYSICAL RESEARCH, VOL. 115, D14206, doi:10.1029/2009JD013086, 2010

Click Here for Full Article

On the spectral dependence of backscatter from cirrus clouds: Assessing CALIOP's 1064 nm calibration assumptions using cloud physics lidar measurements

Mark A. Vaughan,[1] Zhaoyan Liu,[2] Matthew J. McGill,[3] Yongxiang Hu,[1] and Michael D. Obland[1]

Received 26 August 2009; revised 25 February 2010; accepted 15 March 2010; published 28 July 2010.

[1] Recent space-based lidar missions rely on assumptions about the spectral dependence of the backscatter signals from cirrus clouds to calibrate measurements made at 1064 nm. In particular, the calibration procedure employed by the Cloud Aerosol Lidar and Infrared Pathfinder Satellite Observations (CALIPSO) mission assumes that the backscatter color ratio, defined as the ratio of particulate backscatter coefficients at 1064 nm and 532 nm, has a value of 1.00, with an expected standard deviation on the order of 0.04. This work assesses the accuracy of this assumption, and its implications for the CALIPSO 1064 nm calibration scheme, using over 400 h of lidar measurements acquired in the northern hemisphere between 2002 and 2007 by the Cloud Physics Lidar (CPL). For the strongly scattering cirrus clouds typically used for CALIPSO calibrations, the uncorrected CPL-derived backscatter color ratio is 0.83 ± 0.19. Accounting for computational biases introduced by the CPL assumption of pristine air in the calibration region yields a best estimate cirrus cloud color ratio of 1.01 ± 0.25.

Citation: Vaughan, M. A., Z. Liu, M. J. McGill, Y. Hu, and M. D. Obland (2010), On the spectral dependence of backscatter from cirrus clouds: Assessing CALIOP's 1064 nm calibration assumptions using cloud physics lidar measurements, *J. Geophys. Res.*, *115*, D14206, doi:10.1029/2009JD013086.

1. Introduction

[2] Since its launch in April 2006, the Cloud Aerosol Lidar and Infrared Pathfinder Satellite Observations (CALIPSO) mission [*Winker et al.*, 2009] has delivered global and near-continuous measurements of the vertical structure of the Earth's atmosphere. The wealth of information available from this new data set has inspired a renewed search for well-characterized scattering targets that can be used for accurate instrument calibration. CALIPSO, like its predecessors the Lidar In-space Technology Experiment (LITE) [*Winker et al.*, 1996] and the Geoscience Laser Altimetry Satellite (GLAS) [*Spinhirne et al.*, 2005], utilizes a Nd:YAG laser transmitter, and thus calibration concerns have so far focused almost exclusively on the fundamental Nd:YAG wavelength (1064 nm) and its first and second harmonics (532 nm and 355 nm, respectively). For the two shorter wavelengths, the molecular atmosphere in the mid-to-upper stratosphere supplies a reliable calibration target [*Osborn*, 1998; *Reagan et al.*, 2002; *Palm et al.*, 2004]. Air molecules are relatively efficient scatterers at 355 nm and 532 nm, and their backscattering and extinction characteristics are well known, both from theory and in practice [*Bucholtz*, 1995; *Bodhaine et al.*, 1999]. However, because the molecular backscattering cross section is smaller at 1064 nm than at 532 nm by a factor of ~16, the diminished signal levels from the stratosphere make this region a much less appealing calibration target at 1064 nm. Space-based systems are further disadvantaged by the long range from the lidar to the calibration target, and by the mass and power restrictions imposed on space-based platforms. Taken together, these conditions can severely limit the signal-to-noise ratio (SNR) that can be achieved for measurements of weakly scattering targets [*Hunt et al.*, 2009].

[3] The fallback position chosen by all space-based lidars to date is to calibrate the 1064 nm channel using the backscatter from nonmolecular targets having well-known and well-characterized scattering signals. Over the years, several different approaches have been proposed and tried. Prior to the launch of LITE, *Reagan and Zielinskie* [1991] developed a technique that targeted uniform surfaces in the deserts of California. This approach proved reasonably effective, with the retrieved calibration coefficients having uncertainties estimated to be on the order of ~10% [*Reagan et al.*, 2002]. However, opportunities for the application of this method are restricted by the availability of well-characterized sites that lie along the satellite orbit track. *Menzies et al.* [1998] used the ratio of ocean surface reflectances at 532 nm and 1064 nm to calibrate the LITE

[1]Climate Science Branch, NASA Langley Research Center, Hampton, Virginia, USA.
[2]National Institute of Aerospace, Hampton, Virginia, USA.
[3]Mesoscale Atmospheric Processes Branch, NASA Goddard Space Flight Center, Greenbelt, Maryland, USA.

Copyright 2010 by the American Geophysical Union.
0148-0227/10/2009JD013086

1064 nm channel relative to the 532 nm channel, which in turn was directly calibrated via molecular normalization. A comprehensive scheme for lidar calibration using liquid water clouds was proposed by *O'Connor et al.* [2004]. Subsequent refinements were suggested by *Hu et al.* [2006], and the effectiveness of the technique has since been demonstrated using CALIPSO measurements [*Hu et al.*, 2007].

[4] Despite the promise they hold, there are drawbacks to calibration via techniques that use surface measurements and/or liquid water clouds. In particular, these methods all require a cloud-free atmosphere above the target. Furthermore, those methods that calibrate the 1064 nm channel relative to the 532 nm channel require an additional assumption about the spectral dependence of the aerosol optical depth within the measurement column. Successful application of these techniques can thus require substantial spatial and optical analysis before the essential process of calibration can be attempted. To circumvent these limitations, the CALIPSO and GLAS missions have both chosen to calibrate their 1064 nm measurements using the backscatter from dense cirrus clouds [*Hostetler et al.*, 2005; *Palm et al.*, 2002]. Because the scattering from cirrus clouds is assumed to be well characterized, the 1064 nm signals are calibrated by comparison to simultaneous observations acquired by the calibrated 532 nm channel. The strong backscatter from dense cirrus offers a readily identifiable target that ensures high SNR for the calibration measurement. Furthermore, because cirrus clouds exist high in the troposphere, spectral differences in aerosol attenuation are minimized, simply because the atmospheric column above the clouds is largely free of aerosols.

[5] The fundamental assumption motivating the initial development of the cirrus calibration method is that both the backscatter and the extinction coefficients for sufficiently large cirrus particles are spectrally independent; that is, at any range bin, the ratio of cloud backscatter coefficients and the ratio of cloud extinction coefficients will both equal unity [*Reagan et al.*, 2002]. That the extinction coefficients are spectrally independent for large particles measured in the Nd:YAG wavelength regime has long been established [e.g., *Bohren and Huffman*, 1983; *Kent et al.*, 1997; *Beyerle et al.*, 2001]. However, the same cannot be said with equal authority for the backscatter coefficients. In this work we use measurements made by the airborne Cloud Physics Lidar (CPL [*McGill et al.*, 2002]) to assess the spectral dependence of cirrus cloud backscatter coefficients and to explore the continued feasibility of using dense cirrus clouds for space-based lidar calibration. Like CALIPSO and GLAS, CPL is an elastic backscatter lidar, operating at multiple wavelengths. Because CPL typically flies aboard NASA's high-altitude ER2 research aircraft following a straight and level flight plan at ~20 km cruising altitude, it is especially well suited for assessing the spatial and optical properties of cirrus. The substantially higher signal-to-noise ratio of the CPL data allows for calibration of the 1064 nm channel using the well-established molecular normalization technique [*McGill et al.*, 2003]. Analysis of the CPL data sets can therefore provide the independent evaluation of cirrus cloud backscatter color ratios that is required to validate fundamental components of the calibration schemes employed by the current generation of space-based lidars.

[6] The goal of this paper is to establish a measurement-based best estimate of the mean backscatter color ratio of cirrus cloud layers. Our motivation is straightforward: accurate calibration of the CALIPSO 1064 nm lidar data relies critically on knowledge of this value and on an understanding of its natural variability. We begin our work with an overview of color ratio terminology and a review of the cirrus cloud color ratio measurements reported in earlier studies. We then describe the algorithm used to calibrate the CALIPSO 1064 nm lidar data, emphasizing the central role played by the backscatter color ratio of cirrus clouds. After identifying several fundamental assumptions used in the analysis of elastic backscatter lidar data, we briefly review those aspects of the CPL instrument and retrieval algorithms that are especially germane to the measurement of backscatter color ratios in cirrus clouds. Our focus then switches to an analysis of the color ratio distribution derived from the CPL measurements. In particular, we examine the CPL calibration procedures in order to understand and quantify any biases that may be introduced into the cirrus cloud measurements by assumptions made about the aerosol content within the CPL molecular normalization region. Using data from multiple satellites, we assess the aerosol loading in the normalization region during the CPL measurement campaigns. On the basis of our conclusions from this assessment, we apply a parameterized correction factor the CPL data to derive a mean cirrus cloud color ratio of 1.01 ± 0.25. To test the broader applicability of our calibration correction procedure, we apply the same technique to results obtained by other researchers. The paper concludes with a preliminary assessment of the CALIPSO 1064 nm calibration uncertainties that result from our revised evaluation of the backscatter color ratio of cirrus clouds and with some closing remarks that summarize our findings.

2. Color Ratio Terminology

[7] Within the context of elastic backscatter lidar measurements, the concept of a backscatter color ratio is a natural outgrowth of the terms found in the lidar equation, given by

$$P_\lambda(r) = \frac{E_\lambda G_\lambda C_\lambda}{r^2}\left(\beta_{p,\lambda}(r) + \beta_{m,\lambda}(r)\right) T^2_{p,\lambda}(r) T^2_{m,\lambda}(r) T^2_{O_3,\lambda}(r). \quad (1)$$

Here the subscript λ represents the wavelength at which the measurement is made, and the subscripts p, m, and O_3 represent, respectively, contributions to the signal from particulates (i.e., clouds and aerosols), air molecules, and ozone. $P_\lambda(r)$ is the range resolved, background-subtracted signal measured by the lidar at wavelength λ, while C_λ represents the wavelength-specific calibration coefficient. Similarly, E_λ and G_λ quantify the energy emitted by the laser transmitter and the electronic gain of the lidar receiver, respectively. $T^2_{x,\lambda}$ (r) describes the two-way attenuation of the transmitted laser pulse by the various scattering and absorbing constituents of the atmosphere, and is related to the range-dependent volume extinction coefficient by

$$T^2_{x,\lambda}(r) = \exp\left(-2\eta_{x,\lambda}(r)\int_{r_0}^{r}\sigma_{x,\lambda}(r)\,dr\right), \quad (2)$$

where $\sigma_{x,\lambda}$ (r) is the extinction coefficient for constituent x, and $\eta_{x,\lambda}$ (r) is a factor that accounts for multiple scattering [*Winker*, 2003]. For molecular scattering, we assume $\eta_{m,\lambda}$ (r) = 1 (i.e., no contributions from multiple scattering). For particulate scattering, $0 < \eta_{p,\lambda}(r) \leq 1$. The backscatter coefficient for each scattering species within the measurement volume is given by $\beta_{x,\lambda}$ (r). We therefore define the particulate backscatter color ratio χ as the ratio of the particulate backscatter coefficients measured at any two different wavelengths. In our formulation, the measurement at the longer wavelength is always in the numerator of the fraction, so that

$$\chi(r) = \frac{\beta_{p,\lambda_{longer}}(r)}{\beta_{p,\lambda_{shorter}}(r)}. \tag{3}$$

Defined in this way, the color ratio is generally expected to lie between zero and one, with smaller values indicating smaller particles, and $\chi \approx 1$ representing large particles, for which geometric optics should provide an appropriate approximation of the scattering process. Our formulation is not unique, nor is our terminology universally adopted. For example, *Del Guasta and Niranjan* [2001] also use the term "color ratio," but their definition is the inverse of ours. The color ratio defined by *Beyerle et al.* [2001],

$$C(r) = \frac{\beta_{p,\lambda_{longer}}(r)}{\beta_{p,\lambda_{shorter}}(r)}\left(\frac{\lambda_{shorter}}{\lambda_{longer}}\right)^{-4.13} = \chi(r)\left(\frac{\lambda_{shorter}}{\lambda_{longer}}\right)^{-4.13}, \tag{4}$$

augments our definition with an additional term to ensure that the color ratio of particles scattering in the Rayleigh regime is approximately equal to one and that in the large particle regime (i.e., when $\chi(r) \approx 1$), $C(r) \approx 5.32$ at wavelengths of 355 nm and 532 nm, respectively. Finally, *Hair et al.* [2008] and *Su et al.* [2008] express the wavelength dependence of laser backscatter using a "backscatter Ångström exponent" parameter, defined as

$$BAE(r) = \frac{-\ln\left(\beta_{p,\lambda_{longer}}(r)/\beta_{p,\lambda_{shorter}}(r)\right)}{\ln\left(\lambda_{longer}/\lambda_{shorter}\right)} = \frac{-\ln(\chi(r))}{\ln\left(\lambda_{longer}/\lambda_{shorter}\right)}. \tag{5}$$

This formulation has been employed by several other researchers [e.g., *Mattis et al.*, 2003; *Chen et al.*, 2007] and is sometimes referred to as the "color index" [e.g., *Immler and Schrems*, 2003 and *Balis et al.*, 2006].

[8] While measured values of χ for cirrus clouds are only sparsely reported in the extant literature, the few values available are in generally good agreement with one another. *Beyerle et al.* [2001] made lidar measurements of thin cirrus at 355 nm and 532 nm at Table Mountain in southern California (34.4°N, 117.7°W). The color ratio distribution compiled from these data displays a prominent peak at χ = 1, indicative of large particles. The mean value is somewhat lower though, as the distribution is not symmetric, and ~18% of the measurements deviate from the mode by more than 20%. Using measurements made at wavelengths of 532 nm and 1064 nm, *Del Guasta and Niranjan* [2001] report color ratios between 0.5 and 1.0 in the cirrus clouds surrounding contrails over Florence, Italy (43°N). Values within the contrails typically fell within the same range, although some very low values (0.2 to 0.5) were measured in several contrails that displayed unusually low depolarization ratios. This combination of values is interpreted as the signature of micron-sized particles, as, according Del Guasta and Niranjan (and consistent with the Beyerle et al. measurements), ice crystals larger than ~10 μm in size should show a color ratio in the neighborhood of 1. This assertion is in agreement with the results of *Immler et al.* [2007], who report color ratios of approximately 1 for an extensive set of Raman measurements of optically thin tropical cirrus measured in Suriname (5.8°N, 55.2°W). More recently, *Tao et al.* [2008] published a distribution of cirrus cloud color ratios measured by the Hampton University (HU) lidar located in Hampton, Va (37.0°N, 76.3°W). The Tao distribution has a peak value of 0.88, a spread (full width, half maximum) of 0.12, and appears to be somewhat more symmetric and more nearly monomodal than the distribution measured by Beyerle.

3. Overview of the CALIPSO 1064 nm Calibration Algorithm

[9] A full description of the CALIPSO 1064 nm calibration procedure is given in the CALIPSO lidar level 1 algorithm theoretical basis document (*Hostetler et al.* [2005]). Here we provide a brief overview of the process to highlight the importance of obtaining an accurate estimate of χ_{cirrus}.

[10] The 1064 nm calibration coefficients used in the CALIPSO data processing are derived via a relative calibration with respect to the already calibrated 532 nm signal. The calibration transfer equation is

$$C_{1064} = C_{532}\chi_{cirrus}^{-1}\left(\frac{\langle X'_{1064}\rangle}{\langle X'_{532}\rangle}\right). \tag{6}$$

The angle brackets indicate averaging over some (variable) number of consecutive range bins, and

$$X'_{\lambda}(r) = \frac{X_{\lambda}(r)}{T^2_{m,\lambda}(r)T^2_{O_3,\lambda}(r)} = C_{\lambda}\left(\beta_{p,\lambda}(r) + \beta_{m,\lambda}(r)\right)T^2_{p,\lambda}(r)$$
$$\text{for } X_{\lambda}(r) = \frac{r^2 P_{\lambda}(r)}{E_{\lambda}G_{\lambda}}. \tag{7}$$

The components of $X_{\lambda}(r)$, i.e., r, $P_{\lambda}(r)$, E_{λ}, and G_{λ}, are all measured values. The $T^2_{m,\lambda}$ (r) and $T^2_{O_3,\lambda}$ (r) values required to form X'_{λ} (r) are derived from meteorological model data provided by NASA's Global Modeling and Assimilation Office (GMAO) [*Bloom et al.*, 2005]. The 532 nm calibration coefficient C_{532} is estimated using the well-established molecular normalization technique [*Russell et al.*, 1979; *Powell et al.*, 2009]. Once C_{532} has been determined for a set of profile measurements, the 532 nm attenuated scattering ratios are computed for all altitudes below the calibration region (34 to 30 km), using

$$R'_{532}(r) = \frac{X'_{532}(r)}{C_{532}\,\beta_{m,532}(r)} = \left(1 + \frac{\beta_{p,532}(r)}{\beta_{m,532}(r)}\right)T^2_{p}(r), \tag{8}$$

with the molecular backscatter coefficients, $\beta_{m,532}(r)$ being derived from GMAO molecular number density profiles. The R'_{532} profile is then scanned over an altitude range of

17 to 8 km to identify the first occurrence of three or more consecutive range bins for which R'_{532} (r) > 50. Any such region is assumed to be a cirrus cloud, and all range bins meeting the scattering ratio intensity criteria are used to compute $\langle X'_{532}\rangle$ and $\langle X'_{1064}\rangle$. No acceptance testing of any kind is levied on the 1064 nm signals within the calibration region.

[11] From equation (6), the uncertainty in an estimate of C_{1064} derived from a single cirrus cloud measurement is

$$\left(\frac{\Delta C_{1064}}{C_{1064}}\right)^2 = \left(\frac{\Delta C_{532}}{C_{532}}\right)^2 + \left(\frac{\Delta\langle X'_{532}\rangle}{\langle X'_{532}\rangle}\right)^2 + \left(\frac{\Delta\langle X'_{1064}\rangle}{\langle X'_{1064}\rangle}\right)^2 + \left(\frac{\Delta\chi_{\text{cirrus}}}{\chi_{\text{cirrus}}}\right)^2 \quad (9)$$

[*Bevington and Robinson*, 1992]. Pre-launch assessments of the components of the error were $\Delta C_{532}/C_{532} \approx 0.05$, $\Delta\langle X'_{532}\rangle/\langle X'_{532}\rangle \approx 0.054$, $\Delta\langle X'_{1064}\rangle/\langle X'_{1064}\rangle \approx 0.054$, and $\Delta\chi_{\text{cirrus}}/\chi_{\text{cirrus}} \approx 0.04$, for a predicted uncertainty of $\Delta C_{1064}/C_{1064} \approx 0.097$ [*Reagan et al.*, 2002]. Post-launch validation studies have confirmed that $\Delta C_{532}/C_{532} \approx 0.05$ [*Powell et al.*, 2009], and the SNR for all measurement channels is significantly better than was predicted [*Hunt et al.*, 2009]. Completing a post-launch analysis of the uncertainties in the CALIPSO 1064 nm calibration coefficients should thus require only an assessment of the uncertainties in the color ratio term.

[12] Calibration quality cirrus (i.e., those of sufficient backscatter intensity) cannot be guaranteed to occur at regular intervals. Therefore, rather than compute and apply intermittent estimates of C_{1064} using individual cirrus clouds, the operational CALIOP calibration algorithm instead accumulates a sequence of estimates of the calibration scale factor

$$f_i = \chi_{\text{cirrus}}^{-1}\left(\frac{\langle X'_{1064}\rangle}{\langle X'_{532}\rangle}\right)_i. \quad (10)$$

Following the completion of each daytime or nighttime granule, a granule mean scale factor $\langle f\rangle$ is computed, and the 1064 nm calibration constants are subsequently derived using

$$C_{1064}(t) = \langle f\rangle C_{532}(t), \quad (11)$$

where t represents the elapsed time from the beginning of the granule for which $\langle f\rangle$ was computed. The uncertainty in C_{1064} is now given by a slightly modified version of equation (9):

$$\left(\frac{\Delta C_{1064}}{C_{1064}}\right)^2 = \left(\frac{\Delta C_{532}}{C_{532}}\right)^2 + \left(\frac{\Delta\langle f\rangle}{\langle f\rangle}\right)^2, \quad (12)$$

where

$$\left(\frac{\Delta\langle f\rangle}{\langle f\rangle}\right)^2 = \frac{1}{N}\left(\frac{\Delta\langle\chi_{\text{cirrus}}\rangle}{\langle\chi_{\text{cirrus}}\rangle}\right)^2 + \frac{1}{N^2}\sum_{k=1}^{N}\left[\left(\frac{\Delta\langle X'_{532}\rangle_k}{\langle X'_{532}\rangle_k}\right)^2 + \left(\frac{\Delta\langle X'_{1064}\rangle_k}{\langle X'_{1064}\rangle_k}\right)^2\right]. \quad (13)$$

The amended version accounts for the fact that $\langle f\rangle$ is an average value derived by measuring some number N of cirrus clouds.

[13] The procedure described above differs somewhat from the technique originally documented in the CALIOP Level I ATBD. In the original method, which was used for Release 1 of the CALIOP data, equation (6) was used to compute a mean 1064 nm calibration constant for each orbit segment. However, the daytime 532 nm calibration from which the 1064 nm calibration is derived was subsequently found to be time varying function of orbit elapsed time, with variations being attributed to thermally-induced beam steering effects [*Powell et al.*, 2008]. Computing a mean scale factor, rather than a mean calibration coefficient, permits the 1064 nm calibration to vary in the same manner as the 532 nm calibration. The revised scheme described here was introduced beginning with CALIOP Data Release 2.

[14] In closing this section, we note that the assumed spectral independence of laser backscatter from clouds has a long, albeit not especially well-documented, history in the ground-based lidar community. During the International Cirrus Experiment in 1989 at Nordholz, Germany (53.8°N, 8.7°E), *Ansmann et al.* [1993] observed an essentially flat (with respect to altitude) signal ratio profile for uncalibrated backscatter measurements of cirrus clouds acquired at 550 nm and 728 nm. Assuming a value of 1 for this flat region allowed the authors to estimate an aerosol scattering ratio of 1.05 in the upper troposphere. As this value was consistent with other estimates in the literature, they concluded that the scattering from cirrus was spectrally independent. This conclusion was later referenced by *Althausen et al.* [2000] to support the use of a cirrus cloud color ratio of 1 to calibrate the 1064 nm channel of their 6-wavelength, 11-channel system. *Schneider and Eixmann* [2002] also report using an assumed color ratio of 1 for cirrus clouds to calibrate their 1064 nm channel. Taking a slightly different tack, *Sugimoto et al.* [2001] calibrated the 1064 nm data by assuming a color ratio of 1 for water clouds for the 2-channel lidar aboard the Japanese research ship Mirai.

4. Fundamental Retrieval Assumptions

[15] Deriving profiles of particulate backscatter coefficients from elastic backscatter lidar measurements requires knowledge of the range-resolved extinction-to-backscatter ratio (AKA lidar ratio),

$$S_{p,\lambda}(r) = \sigma_{p,\lambda}(r)/\beta_{p,\lambda}(r). \quad (14)$$

[16] Unlike Raman systems [*Ansmann et al.*, 1992] and high spectral resolution lidars (HSRL) [*Grund and Eloranta*, 1990], the measurements made by elastic backscatter lidars do not contain sufficient information to permit the retrieval of $S_{p,\lambda}$ (r). Consequently, in the analysis of data obtained using these instruments, values of the mean layer lidar ratio are typically estimated (or assumed) based on some a priori considerations of layer type [e.g., *McGill et al.*, 2003; *Atlas et al.*, 2006; *Omar et al.*, 2009]. Exceptions to the requirement for an assumed lidar ratio occur on those occasions when a measurement of layer optical depth is available. In

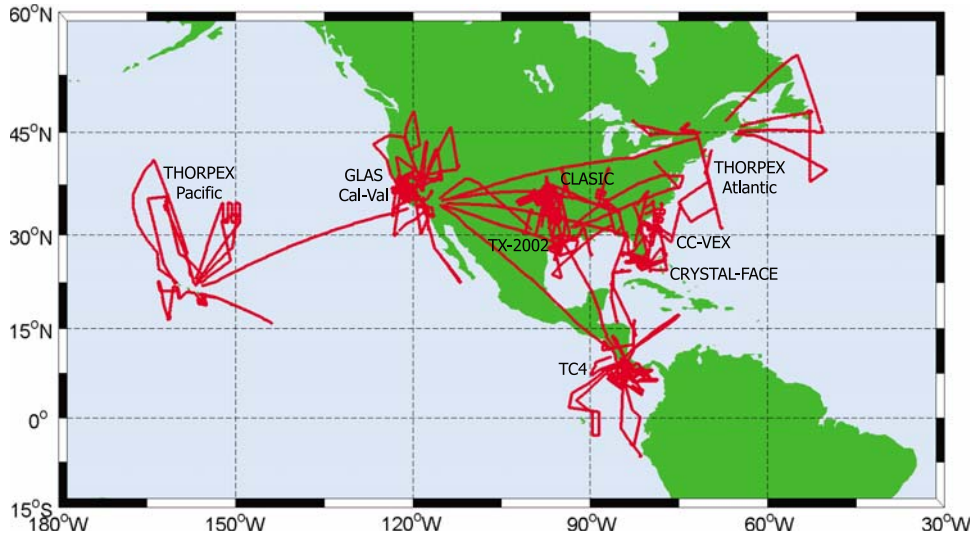

Figure 1. CPL flight tracks for all data included in this study.

such cases, a layer effective lidar ratio can be retrieved directly from the data [*Young*, 1995].

[17] As particle sizes approach the geometric optics regime, the spectral dependence of the extinction coefficients will vanish [*Bohren and Huffman*, 1983]. For the size distributions characteristic of cirrus clouds, we can reasonably assume that the extinction color ratio $\alpha(r) = \sigma_{p,1064}(r)/\sigma_{p,532}(r)$ measured by both CPL and CALIPSO is effectively unity and that cirrus optical depths are identical at both wavelengths. By enforcing this assumption, we can use range-resolved lidar ratios to derive a second expression for the particulate backscatter color ratio:

$$\left(\frac{S_{532}(r)}{S_{1064}(r)}\right)_{cirrus} = \left(\frac{\sigma_{532}(r)}{\beta_{532}(r)}\right)\left(\frac{\beta_{1064}(r)}{\sigma_{1064}(r)}\right) = \chi_{cirrus}(r). \qquad (15)$$

Similarly, for the layer effective lidar ratios, we can measure using elastic backscatter lidars

$$\left(\frac{S_{532}}{S_{1064}}\right)_{cirrus} = \left(\frac{\tau_{532}}{\gamma_{532}}\right)\left(\frac{\gamma_{1064}}{\tau_{1064}}\right) = \chi_{cirrus}, \qquad (16)$$

where τ is cirrus cloud optical depth, γ is the layer integrated particulate backscatter, and χ_{cirrus} is the layer effective backscatter color ratio.

5. CPL Measurements

5.1. CPL Data Analysis Algorithms

[18] The Cloud Physics Lidar is polarization-sensitive, elastic backscatter lidar equipped with a Nd:YVO_4 laser-emitting pulsed laser light at wavelengths of 355, 532, and 1064 nm. A complete description of the instrument, including full specifications for both the transmitter and the receiver, is given by *McGill et al.* [2002]. Here we will review only those aspects of the CPL that are relevant to the color ratio measurement. Our primary concern is with the methods and quality of the lidar calibration, as obtaining accurate values of χ_{cirrus} depends critically on having an accurately calibrated lidar. Because CPL is a nadir-viewing system flying in the lower stratosphere, it can reliably calibrate all three wavelengths using the molecular normalization technique [*McGill et al.*, 2003]. Because the aerosol content of the upper troposphere is generally lower than is typical of the middle and lower altitudes [*Thomason and Peter*, 2006], the accuracy of the standard CPL calibration product should be somewhat better than would be expected of zenith-viewing elastic backscatter lidars employing the same technique at lower altitudes. Cloud and aerosol layers in the CPL data are detected using an adaptive thresholding technique that compares the current signal levels to estimates of the localized mean "clear air" signal. The mechanics of the layer detection and cloud-aerosol discrimination algorithms are essentially identical to those used by GLAS but with adjustments made to account for instrument-specific differences [*Palm et al.*, 2002; *Hart et al.*, 2005]. Extinction profiles are subsequently derived for each layer identified by applying a two component Fernald-like algorithm to the calibrated backscatter data [*Fernald*, 1984; *McGill et al.*, 2003].

5.2. Measurement Locations

[19] Over the past decade, CPL has participated in numerous long-duration field campaigns and acquired an extensive database of cirrus cloud measurements. In this study we will use data from the Cirrus Regional Study of Tropical Anvils and Cirrus Layers - Florida Area Cirrus Experiment (CRYSTAL-FACE), the 2002 Terra-Aqua experiment (TX-2002), the Observing-System Research and Predictability Experiment (THORPEX), the CALIPSO-CloudSat Validation Experiment (CC-VEX), the Cloud and Land Surface Interaction Campaign (CLASIC), and the Tropical Composition, Cloud and Climate Coupling experiment (TC4). The specific measurement objectives of these different missions were widely varied and include studies of cirrus anvils and their associated convective systems (CRYSTAL-FACE) [*McGill et al.*, 2004], validation of numerical weather prediction schemes (THORPEX) [*Zhou et al.*, 2005], observations of cumulus convection (CLASIC) [*Miller*, 2008], and the tropical upper troposphere and tropopause transitional layer (TC4) [*DeSlover et al.*, 2007],

Table 1. Cloud Physics Lidar Field Campaigns Used to Derive Spatial and Optical Statistics[a]

Mission	Dates	Latitude Range
CRYSTAL-FACE	July 2002	14°N–29°N
TX-2002	November–December 2002	26°N–38°N
THORPEX-Pacific	February–March 2003	16°N–40°N
GLAS Cal-Val	October 2003	33°N–47°N
THORPEX-Atlantic	November–December 2003	32°N–53°N
CC-VEX	July–August 2006	23°N–40°N
CLASIC	June 2007	28°N–40°N
TC4	July–August 2007	3°N–39°N

[a]Data were compiled from all flights during each campaign, excluding only those for which the measurements were compromised by an instrument malfunction.

and calibration validation flights for GLAS (GLAS Cal-Val) [*Hlavka et al.*, 2005] and CALIPSO (CC-VEX) [*McGill et al.*, 2007]. During these campaigns, CPL acquired cirrus cloud measurements at latitudes between 4°N and 52°N and over longitudes from Nova Scotia westward to the Hawaiian Islands. Altogether, over 400 h of data have been collected and analyzed. The dates and locations of all campaigns utilized in this study are summarized in Table 1. Flight tracks are shown in Figure 1.

5.3. Data Selection and Analysis

[20] For semitransparent cirrus, χ_{cirrus} can be derived directly from the CPL data products using equation (16), and thus, our initial analysis focuses on these layers. CPL derives lidar ratios at 532 and 1064 nm by constraining the extinction retrieval using optical depth estimates obtained from analysis of clear air regions immediately above and below the cloud layers [*Young*, 1995; *McGill et al.*, 2003]. Measurements of layer two-way transmittance are made at 532 nm. The lidar ratios at 1064 are retrieved by assuming that cirrus clouds consist predominantly of large particles, and thus, the cloud optical depths are identical at both wavelengths. This tactic is necessary because, due to signal attenuation and the relative insensitivity of the 1064 nm channel to molecular scattering, the 1064 nm SNR on the far side of the cloud is too low to permit reliable estimates of optical depth even for clouds of only moderate optical thickness (e.g., $\tau \leq 0.5$).

[21] Constrained lidar ratio retrievals can be unreliable for weakly scattering layers with low optical depths. Therefore, to ensure robust retrievals, the following requirements were imposed on all layers selected for this study: (1) only the uppermost layer in any profile was considered; (2) the layer mean depolarization ratio $\delta_{1064} = \beta_{\perp,1064}/\beta_{\|,1064}$ was required to exceed 0.2, thus, ensuring that candidate clouds are much more likely to be ice, not water [*Sassen and Benson*, 2001]; and (3) a minimum value of 0.015 sr^{-1} was levied on the 532 nm integrated attenuated total backscatter (see equation (18)). Using these selection criteria yielded a sample population of 13,332 layers. The mean optical depth of these semitransparent layers was 0.77 ± 0.35. The layer-effective backscatter color ratio, derived using equation (15), was 0.82 ± 0.13, which is consistent with the value reported by *Tao et al.* [2008]. Descriptive statistics for selected optical parameters derived from this data set are shown in Table 2. The distribution of color ratio values is depicted in Figure 2. The width of the distribution is a function of both natural variability and the uncertainties associated with the constrained retrievals of the lidar ratios at both channels (e.g., see *Young* [1995] and/or *Del Guasta* [1998]).

[22] This analysis of semitransparent layers is perhaps not sufficient to establish a mean color ratio value to be used in

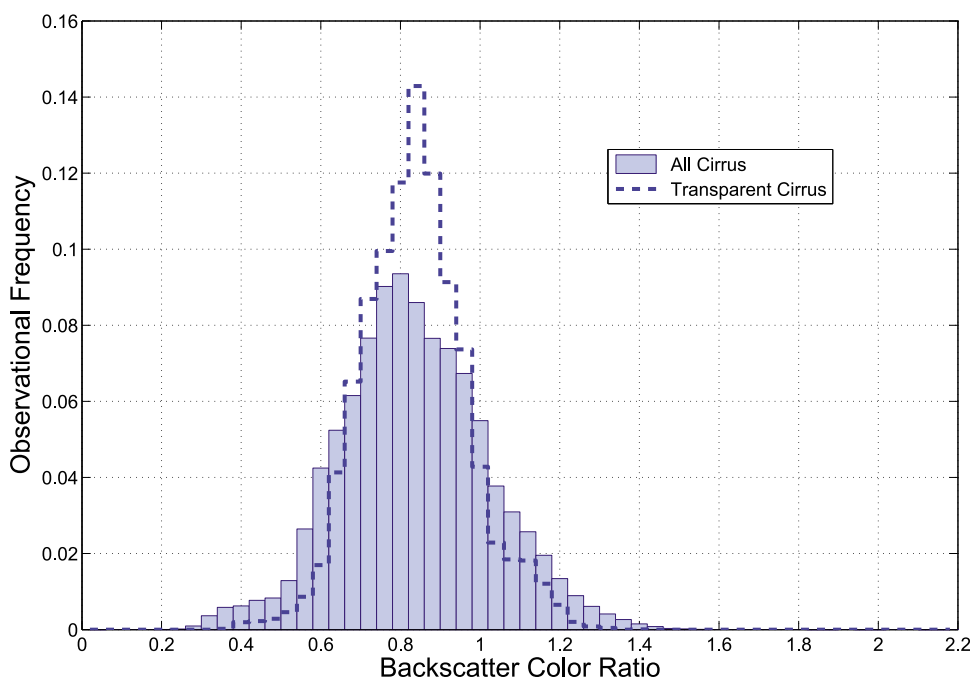

Figure 2. Distributions of χ derived from transparent cirrus only (dashed line) and from opaque and transparent cirrus combined (solid bars).

Table 2. Scattering Statistics for 13,332 Semitransparent Layers Measured by Cloud Physics Lidar in the Northwest Hemisphere Between 2002 and 2007[a]

Quantity	Minimum	Maximum	Median	Mean	Standard Deviation
γ'_{532} (sr^{-1})	0.0150	0.0386	0.0182	0.0193	0.0039
δ_{1064}	0.200	0.691	0.476	0.465	0.101
τ_{532}	0.232	2.33	0.702	0.768	0.349
S_{532} (sr)	12.0	31.0	19.1	19.2	4.02
S_{1064} (sr)	12.0	52.4	23.4	24.0	6.03
$\chi_{\mathrm{cirrus}} = S_{532}/S_{1064}$	0.349	1.38	0.814	0.817	0.133

[a]Minimum values of γ'_{532} and δ_{1064} were fixed by the layer selection criteria.

the operational CALIPSO 1064 nm calibration scheme. One might hypothesize that the size distributions of the ice crystals within these clouds could be skewed toward smaller mean values. Such behavior would be expected, for example, of the contrail cirrus measured by *Del Guasta and Niranjan* [2001]. The CALIPSO approach implicitly recognizes this possibility by restricting the 1064 nm calibration to those clouds having 532 nm attenuated scattering ratios that consistently exceed 50 [*Hostetler et al.*, 2005]. Within the CPL data set, a large fraction of the clouds that meet the CALIPSO scattering ratio requirement are opaque. However, since opaque cirrus cannot be analyzed using a constrained lidar ratio retrieval, alternate approaches must be formulated. One such approach is to use the ratio of the integrated attenuated backscatters. This quantity is computed using the "particulate-attenuated total backscatter coefficient," given by

$$\mathsf{B}_\lambda(\mathrm{r}) = \frac{\mathrm{X}'_\lambda(\mathrm{r})}{\mathrm{C}_\lambda} = \left(\beta_{\mathrm{p},\lambda}(\mathrm{r}) + \beta_{\mathrm{m},\lambda}(\mathrm{r})\right)\mathrm{T}^2_{\mathrm{p},\lambda}(\mathrm{r}). \tag{17}$$

Integrating this quantity from layer top to layer base yields

$$\begin{aligned} \mathcal{g}'_\lambda &= \int_{\mathrm{top}}^{\mathrm{base}} \mathsf{B}_\lambda(\mathrm{r})\,\mathrm{dr} = \int_{\mathrm{top}}^{\mathrm{base}} \left(\beta_{\lambda,\mathrm{p}}(\mathrm{r}) + \beta_{\lambda,\mathrm{m}}(\mathrm{r})\right)\mathrm{T}^2_{\lambda,\mathrm{p}}(\mathrm{r})\,\mathrm{dr} \\ &= \int_{\mathrm{top}}^{\mathrm{base}} \beta_{\lambda,\mathrm{p}}(\mathrm{r})\mathrm{T}^2_{\lambda,\mathrm{p}}(\mathrm{r})\,\mathrm{dr} + \int_{\mathrm{top}}^{\mathrm{base}} \beta_{\lambda,\mathrm{m}}(\mathrm{r})\mathrm{T}^2_{\lambda,\mathrm{p}}(\mathrm{r})(\mathrm{r})\,\mathrm{dr}. \end{aligned} \tag{18}$$

The quantity of primary interest is the particulate-only integrated attenuated backscatter term

$$\gamma'_\lambda = \int_{\mathrm{top}}^{\mathrm{base}} \beta_{\lambda,\mathrm{p}}(\mathrm{r})\mathrm{T}^2_{\lambda,\mathrm{p}}(\mathrm{r})\,\mathrm{dr}, \tag{19}$$

which can be readily approximated numerically using

$$\begin{aligned} \mathcal{g}'_\lambda &\approx \frac{1}{2}\sum_{\mathrm{k=top+1}}^{\mathrm{base}} (\mathrm{z}_{\mathrm{k-1}} - \mathrm{z}_{\mathrm{k}})\left(\mathsf{B}_{\lambda,\mathrm{k-1}} + \mathsf{B}_{\lambda,\mathrm{k}}\right) \\ \Delta\mathcal{g}'_\lambda &= \frac{1}{2}\left(\mathrm{z}_{\mathrm{top}} - \mathrm{z}_{\mathrm{base}}\right)\left(\mathsf{B}_{\lambda,\mathrm{top}} + \mathsf{B}_{\lambda,\mathrm{base}}\right) \\ \gamma'_\lambda &= \mathcal{g}'_\lambda - \Delta\mathcal{g}'_\lambda \end{aligned} \tag{20}$$

[*Vaughan et al.*, 2005]. For totally attenuating clouds,

$$\gamma'_\lambda = \frac{1}{2\overline{\eta}_\lambda \mathrm{S}_\lambda}, \tag{21}$$

where $\overline{\eta}_\lambda$ is the layer-effective multiple scattering factor [*Platt*, 1973]. Therefore, assuming that the spectral differences in multiple scattering are negligible for cirrus clouds (a well-founded assumption for the CPL measurements [*McGill et al.*, 2002; *Noel et al.*, 2004]), the ratio of the integrated attenuated backscatters provides an approximation for the particulate backscatter color ratio according to

$$\frac{\gamma'_{1064}}{\gamma'_{532}} = \frac{2\,\mathrm{S}_{532}\,\overline{\eta}_{532}}{2\,\mathrm{S}_{1064}\,\overline{\eta}_{1064}} \approx \frac{\mathrm{S}_{532}}{\mathrm{S}_{1064}} = \chi_{\mathrm{cirrus}}. \tag{22}$$

The accuracy of this approximation is readily assessed by comparing the color ratios computed using constrained lidar ratio solutions to the corresponding values calculated using equation (22) for the semitransparent cloud data set described in Table 2. As shown in Figure 3, the correspondence between the two retrieval techniques is excellent: the correlation coefficient is 0.98, the slope of the line of best fit is 1.00, and the intercept (i.e., the bias term) is less than 0.01.

5.4. CPL Color Ratio Distribution

[23] For the remainder of this work, the color ratios reported are calculated using equation (22), thus, permitting the inclusion of cirrus cloud layers whose scattering magnitudes are more representative of the cirrus used in the CALIPSO calibration algorithm. Retaining the selection criteria given in section 5.3 but now expanding the layers considered to also include opaque layers, we increase the sample size by an order of magnitude, to a total of 153,959 layers. While this much larger sample shows some increased variability, the mean measured color ratio is essentially unchanged: $\chi_{\mathrm{cirrus}} = 0.83 \pm 0.19$ for the all cirrus data set versus $\chi_{\mathrm{cirrus}} = 0.82 \pm 0.13$ for the data set restricted to semitransparent cirrus only and derived using equation (16). The distributions from both analyses are shown in Figure 2.

[24] A mean value of χ_{cirrus} that is different from the expected value of 1 would not be fatal to the CALIPSO calibration scheme, as it would be a trivial task to substitute $\chi_{\mathrm{cirrus}} = 0.83$ for the currently assumed value of $\chi_{\mathrm{cirrus}} = 1$. However, the spread of the color ratio distribution suggests that if individual cirrus clouds were used for calibration, a revised cirrus selection technique might be required in order to restrict the range of χ values used, and thus, minimize the uncertainties in the derived coefficients. As shown in Figure 4, this may not be a straightforward task, as there is no strong correlation between χ_{cirrus} and either the extrinsic properties (backscatter intensity, quantified by the 532 nm mean attenuated scattering ratio, $\langle \mathrm{R}'_{532} \rangle$) or the immediately measurable intrinsic properties (depolarization ratio, δ_{1064}) of the layers. χ_{cirrus} and δ_{1064} are essentially uncorrelated ($r = -0.03$), while there is a slight negative correlation ($r = -0.27$) between χ_{cirrus} and the backscatter intensity of the layer.

[25] Figure 5 shows the distribution of all CPL color ratio measurements as a function of latitude, color coded

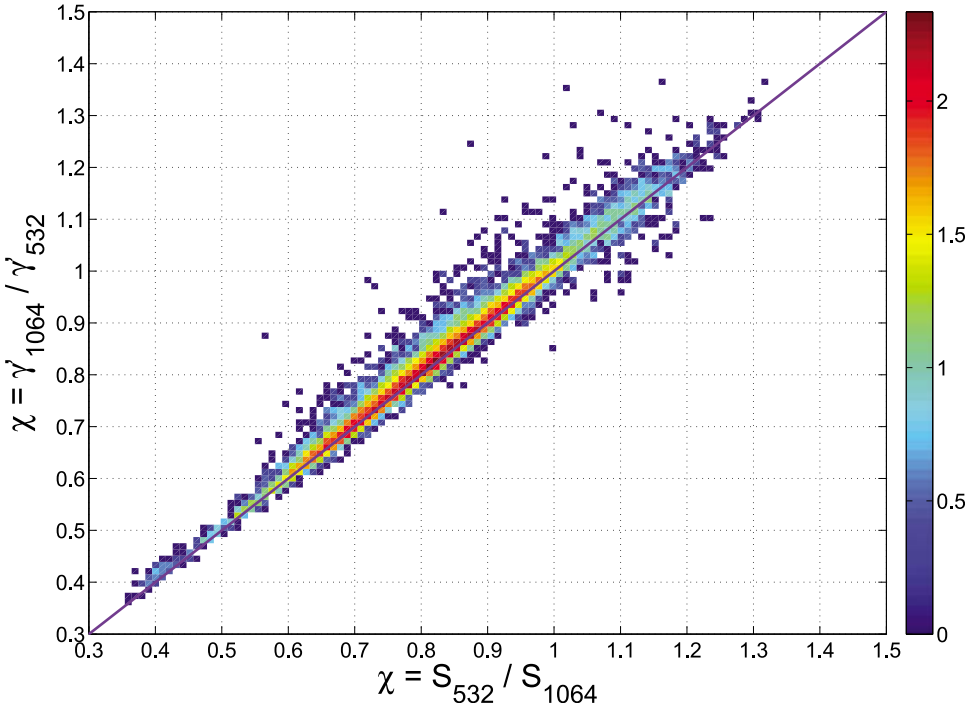

Figure 3. Comparison of analytically derived color ratios (x-axis) to those derived via the integrated attenuated backscatter approximation (y-axis). A color-coded histogram of values shown is for all 13332 transparent layers summarized in Table 2. A log scale is used (e.g., $2 = 10^2 = 100$), with reds indicating more samples, and blues fewer. The data sets have a line of best fit (shown in magenta) of $y = 0.0091 + 1.0016x$, and a correlation coefficient of $r = 0.985$.

according to the field mission during which they were acquired. The values for midlatitude cirrus are seen to be identical to within the error bars (one standard deviation) from ~15°N to ~45°N. Outside that range, the color ratios exhibit somewhat higher values. This is especially true for data acquired in the tropics. For the TC4 mission, when the ER2 flew out of San Jose, Costa Rica (10.0°N, 84.22°W), the mean color ratio was $\chi_{\text{cirrus}} = 1.00 \pm 0.16$. Table 3 provides a synopsis of selected cirrus cloud optical parameters measured during each of the CPL field campaigns. We note in passing that, while the γ'_{532} and δ_{1064} values for the CLASIC and TC4 experiments are astonishingly similar, the color ratios are somewhat different. This fact may have significance for two reasons. First, because these were back-to-back missions (see Table 1), CPL remained mounted on the ER2 for the duration, so changes in measured data cannot be

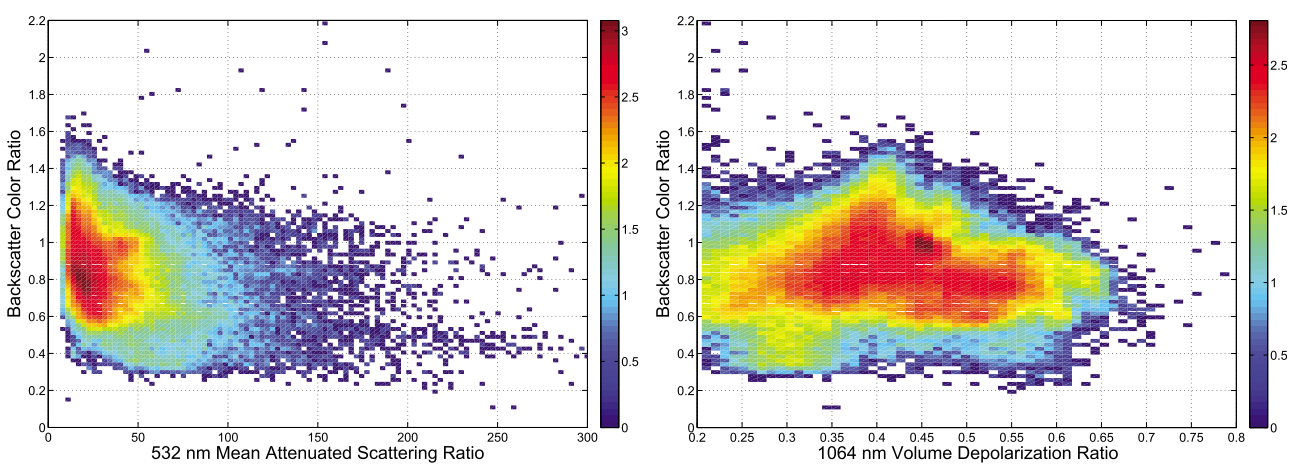

Figure 4. Histograms of χ_{cirrus} as a function of 532 nm backscatter intensity (left) and 1064 nm volume depolarization ratio (right). The color coding in both images uses a logarithmic scale.

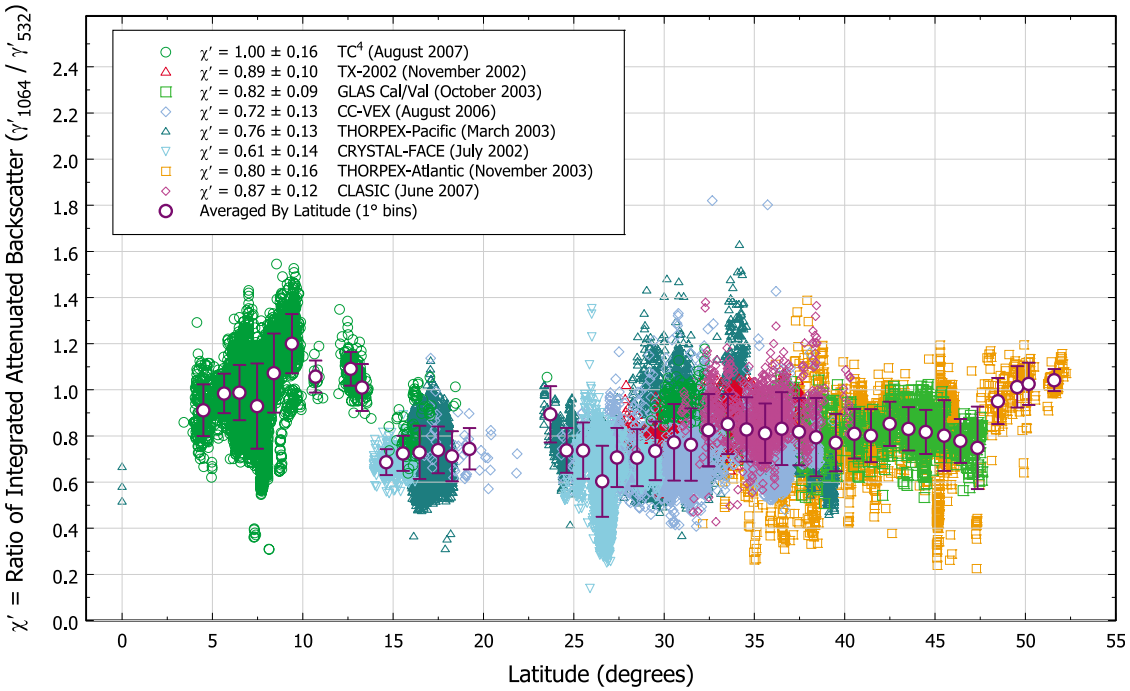

Figure 5. Latitudinal distribution of cirrus cloud color ratios measured by CPL between 2002 and 2007.

attributed to unexplained (and unintended) changes in instrument configuration. Second, the CLASIC flights took place over the interior of the North American continent, while the TC4 flights were all over tropical oceans, leading to speculation color ratio may be a function of cloud type or generating mechanism.

6. CPL Measurement Uncertainties

[26] The distributions of color ratio values shown in Figure 2 includes uncertainties from several sources. The widths of the distributions are influenced both by random errors in the CPL measurements and by the natural variability of cirrus cloud color ratios. The mean values of the distributions may be perturbed due to bias errors that may be inherent in the measurements or introduced by the retrieval scheme. While the effect of random errors can be largely reduced by averaging, this is not so for bias errors, and thus, determining the correct value color ratio to use in the CALIOP calibration scheme requires an assessment of any bias errors that may exist within the CPL retrieval. We begin by applying the mean value theorem for integrals, so that the expression for the integrated attenuated backscatter can be written as

$$\begin{aligned}\gamma'_\lambda &= \int_{top}^{base} B(r)\,dr - \frac{1}{2}\left(B(r_{top}) + B(r_{base})\right)\left(r_{top} - r_{base}\right)\\ &= \frac{\langle X'_\lambda(r)\rangle_{cloud}\left(r_{top} - r_{base}\right)}{C_\lambda} - \frac{\left(X'_\lambda(r_{top}) + X'_\lambda(r_{base})\right)\left(r_{top} - r_{base}\right)}{2\,C_\lambda},\\ &= \frac{\left[\langle X'_\lambda(r)\rangle_{cloud} - \tfrac{1}{2}\left(X'_\lambda(r_{top}) + X'_\lambda(r_{base})\right)\right]\left(r_{top} - r_{base}\right)}{C_\lambda}\end{aligned} \tag{23}$$

where $\langle X'_\lambda(r)\rangle_{cloud}$ is the mean value of $X'_\lambda(r)$ computed over the altitude range from cloud top to cloud base. The backscatter color ratio is thus seen to depend on the ratio of the calibration coefficients for the two channels according to

$$\begin{aligned}\chi &= \frac{\gamma'_{1064}}{\gamma'_{532}}\\ &= \left(\frac{C_{532}}{C_{1064}}\right)\left(\frac{\langle X'_{1064}(r)\rangle_{cloud} - \tfrac{1}{2}\left(X'_{1064}(r_{top}) + X'_{1064}(r_{base})\right)}{\langle X'_{532}(r)\rangle_{cloud} - \tfrac{1}{2}\left(X'_{532}(r_{top}) + X'_{532}(r_{base})\right)}\right).\end{aligned} \tag{24}$$

Table 3. Cloud Statistics for all Cloud Physics Lidar Field Campaigns

Mission	Cloud Top (km)	γ'_{532} (sr^{-1})	δ_{1064}	χ_{cirrus}
CRYSTAL-FACE	13.467 ± 1.351	0.0211 ± 0.0053	0.310 ± 0.049	0.607 ± 0.145
TX-2002	12.217 ± 1.753	0.0240 ± 0.0067	0.399 ± 0.073	0.890 ± 0.097
THORPEX-Pacific	12.160 ± 1.728	0.0223 ± 0.0064	0.425 ± 0.090	0.757 ± 0.135
GLAS Cal-Val	10.982 ± 0.990	0.0227 ± 0.0058	0.511 ± 0.083	0.824 ± 0.094
THORPEX-Atlantic	10.293 ± 2.750	0.0267 ± 0.0110	0.477 ± 0.084	0.802 ± 0.157
CC-VEX	13.514 ± 1.547	0.0196 ± 0.0044	0.441 ± 0.087	0.717 ± 0.130
CLASIC	12.328 ± 1.516	0.0198 ± 0.0040	0.365 ± 0.061	0.873 ± 0.117
TC4	13.922 ± 1.717	0.0198 ± 0.0042	0.368 ± 0.061	1.003 ± 0.162

The CPL calibration coefficients, in turn, are derived by normalizing the measured signal with respect to a molecular backscatter model over some altitude range that is assumed to be free of aerosol contamination. Because CPL is a nadir-viewing system flying in the lower stratosphere, the altitude regime typically used for calibration is in the upper troposphere, near the tropopause. While the aerosol content of this region is generally less than would be found in the lower and middle regions of the troposphere, it still cannot be guaranteed to be aerosol-free and thus may be characterized by a spatially and temporally varying total-to-molecular backscatter ratio R_{cal} greater than 1. The CPL calibration equation, however, estimates a fixed value of $\tilde{\mathrm{R}}_{\mathrm{cal}} = 1$ for all wavelengths and all altitude regimes and latitude bands, so that operational estimates of the calibration coefficients $\tilde{\mathrm{C}}_{\mathrm{CPL},\lambda}$ are derived using

$$\tilde{\mathrm{C}}_{\mathrm{CPL},\lambda} = \frac{\left\langle \mathrm{X}'_{\lambda}(\mathrm{r}) \right\rangle_{\mathrm{cal}}}{\left\langle \beta_{\lambda,\mathrm{m}}(\mathrm{r}) \right\rangle_{\mathrm{cal}}}, \tag{25}$$

where $\langle \mathrm{X}'_{\lambda}\ (\mathrm{r}) \rangle_{\mathrm{cal}}$ represents the average of the sequence of X'_{λ} (r) values computed over the calibration region, and $\beta_{\lambda,\mathrm{m}}$ (r) are the molecular backscatter coefficients, derived from a model or from local rawinsonde soundings. To assess the possible biases introduced into the color ratio estimates by the choice of $\tilde{\mathrm{R}}_{\mathrm{cal}} = 1$, we rewrite the CPL molecular normalization equation as

$$\begin{aligned} \mathrm{C}_{\mathrm{CPL},\lambda} &= \frac{\left\langle \mathrm{X}'_{\lambda}(\mathrm{r}) \right\rangle_{\mathrm{cal}}}{R_{\lambda,\mathrm{cal}} \left\langle \mathrm{T}^2_{\lambda,\mathrm{a}}(\mathrm{r}) \right\rangle_{\mathrm{cal}} \left\langle \beta_{\lambda,\mathrm{m}}(\mathrm{r}) \right\rangle_{\mathrm{cal}}} \\ &= \frac{\tilde{\mathrm{C}}_{\mathrm{CPL},\lambda}}{\mathrm{R}_{\lambda,\mathrm{cal}} \left\langle \mathrm{T}^2_{\lambda,\mathrm{a}}(\mathrm{r}) \right\rangle_{\mathrm{cal}}}, \end{aligned} \tag{26}$$

where $\mathrm{R}_{\lambda,\mathrm{cal}}$ is the actual scattering ratio in the calibration region at wavelength λ, $\langle \mathrm{T}^2_{\lambda,\mathrm{a}}\ (\mathrm{r}) \rangle_{\mathrm{cal}}$ is the mean two-way transmittance because of aerosols in the calibration region, and $\mathrm{C}_{\mathrm{CPL},\lambda}$ is the unbiased estimate of the calibration coefficient that would be used if instantaneous and perfect knowledge of the background aerosol content of the calibration region was available. Substituting equation (26) into equation (24) shows that to derive an unbiased estimate, the measured CPL color ratios must be multiplied by a bias correction term given by

$$\Delta\chi_{\mathrm{CPL.bias}} = \left(\frac{\mathrm{R}_{1064,\mathrm{cal}}}{\mathrm{R}_{532,\mathrm{cal}}} \right) \left(\frac{\left\langle \mathrm{T}^2_{1064,\mathrm{a}}(\mathrm{r}) \right\rangle_{\mathrm{cal}}}{\left\langle \mathrm{T}^2_{532,\mathrm{a}}(\mathrm{r}) \right\rangle_{\mathrm{cal}}} \right). \tag{27}$$

While the ratio of the two-way transmittances in equation 27 is included for completeness, this term contributes essentially nothing to the final value of $\Delta\chi_{\mathrm{CPL.bias}}$. Even with moderate aerosol loading ($R_{532,\mathrm{cal}} \leq 1.05$), the aerosol optical depths of the calibration region will be quite small at both wavelengths, and hence, the ratio of the two-way transmittances will be very close to one. For example, suppose we assume $R_{532,\mathrm{cal}} = 1.05$ in a midlatitude calibration region between 15 and 13 km. Applying the scattering parameters given in Table 2 from *Cattrall et al.* [2005] yields a two-way transmittance ratio between 1.000 and 1.001 for all of the aerosol types listed, thus, demonstrating that the contribution of this term is extremely small.

[27] If the air in the calibration region is truly pristine, then $\mathrm{R}_{532,\mathrm{cal}} = \mathrm{R}_{1064,\mathrm{cal}} = 1$, and there is no calibration bias in the reported values of χ_{CPL}. However, while such conditions may occasionally occur, mean values of $R_{532} = 1$ are not typical. In a comparison of measurements made by multiple satellite-based passive sensors, *Vanhellemont et al.* [2008] found a median 525 nm aerosol extinction coefficient of ~5 × 10^{-4} km^{-1} at an altitude of 15 km in the Northern Hemisphere. An extensive review of the spatial and temporal variability of stratospheric and upper tropospheric aerosols conducted by the Stratospheric Processes And their Role in Climate (SPARC) project reports similar values and, importantly, shows that the mean aerosol extinction magnitudes in the CPL calibration region have been stable from the late 1990s onward [*Thomason and Peter*, 2006]. Because elastic backscatter lidars do not measure extinction directly, converting the extinction measurements by Vanhellemont et al. to an approximate scattering ratio requires some knowledge of the lidar ratio for background aerosols in the upper troposphere/lower stratosphere. Various measured [e.g., *Mattis et al.*, 2004], calculated [e.g., *Ramachandran and Jayaraman*, 2003], modeled [e.g., *Gobbi*, 1995], and assumed [e.g., *Chen et al.*, 2004] estimates for this quantity have been published in the literature, with typical values being in the neighborhood of 50 sr at 532 nm. Taken together, these extinction data and lidar ratio estimates, when combined with molecular number density data from the U.S. Standard Atmosphere, imply that a mean scattering ratio of approximately 1.04 would be an appropriate value for $\mathrm{R}_{532,\mathrm{cal}}$ at 15 km in the Northern Hemisphere.

[28] Both the SPARC report and that of Vanhellemont et al. also provide data on aerosol extinction at 1020 nm. Despite the availability of these data, determining a best estimate for $\mathrm{R}_{1064,\mathrm{cal}}$ is not straightforward, simply because the requisite lidar ratio at 1064 is not well known. We therefore derive an estimate of $\mathrm{R}_{1064,\mathrm{cal}}$ via measured and modeled estimates of the 1064/532 backscatter color ratio of background aerosols $\chi_{\mathrm{a,bkg}}$. During the Global Backscatter Experiment, *Spinhirne et al.* [1997] conducted a rigorous, multiwavelength lidar measurement campaign during which they determined that $\chi_{\mathrm{a,bkg}}$ lay in the range between 0.2 and 0.4. Subsequent modeling results by *Gobbi* [1998] suggest that the upper end of this range is appropriate for those aerosols having 532 nm backscatter coefficients in the range of ~1 × 10^{-5} km^{-1} sr^{-1} (i.e., consistent with the estimate used in deriving $\mathrm{R}_{352,\mathrm{cal}}$ above). If we therefore adopt a value of $\chi_{\mathrm{a,bkg}} = 0.4$ as a calibration standard for 1064 nm measurements [e.g., as in *Hair et al.*, 2008], we can convert values of $\mathrm{R}_{532,\mathrm{cal}}$ into the required value of $\mathrm{R}_{1064,\mathrm{cal}}$ using

$$\mathrm{R}_{1064,\mathrm{cal}} = 1 + \frac{\chi_{\mathrm{a,bkg}}\left(\mathrm{R}_{532,\mathrm{cal}} - 1\right)}{\chi_{\mathrm{m}}}, \tag{28}$$

where χ_{m} is the color ratio for molecular backscatter, such that $\chi_{\mathrm{m}} = \beta_{\mathrm{m},1064}\ (\mathrm{r})/\beta_{\mathrm{m},532}\ (\mathrm{r}) = 2^{-4.05}$ [*Bucholtz*, 1995].

Table 4. Estimates of the Measured Cloud Physics Lidar Color Ratio, $\chi_{cirrus} = 0.83$, Corrected for the Bias Introduced by Assuming Clear Air Scattering Ratios of $R_{532,cal} = R_{1064,cal} = 1$ in the CPL calibration region

$R_{532,cal}$	$R_{1064,cal}$	$E_{CPL,bias}$	Corrected Color Ratio
1.00	1.00	1.00	0.83 ± 0.22
1.01	1.07	1.06	0.88 ± 0.22
1.02	1.13	1.11	0.92 ± 0.23
1.03	1.20	1.16	0.97 ± 0.24
1.04	1.27	1.22	1.01 ± 0.25
1.05	1.33	1.27	1.05 ± 0.27
1.06	1.40	1.32	1.09 ± 0.29
1.07	1.46	1.37	1.14 ± 0.31
1.08	1.53	1.42	1.18 ± 0.33

The bias error in the backscatter color ratio as a function of an assumed value of $\tilde{R}_{cal} = 1$ is thus

$$E_{CPL,bias} = \left(\frac{1}{R_{532,cal}}\right)\left[1 + \left(\frac{\chi_{a,bkg}}{\chi_m}\right)\left(R_{532,cal} - 1\right)\right], \qquad (29)$$

and the unbiased estimate of the CPL cirrus cloud color ratio is $\chi_{corrected} = E_{CPL,bias} \cdot \chi_{CPL,measured}$. In this derivation, the correction applied to the CPL measurements of χ_{cirrus} depends on both the aerosol loading ($R_{532,cal}$) and the color ratio of the backscatter aerosols ($\chi_{a,bkg}$) in the CPL calibration region. Rescaling χ_{cirrus} by application of equation (29) introduces an additional uncertainty in the corrected values given by

$$\Delta E_{CPL,bias} = \sqrt{\left(\frac{\chi_{a,bkg} - \chi_m}{\chi_m R_{532,cal}}\right)^2 \left(\frac{\Delta R_{532,cal}}{R_{532,cal}}\right)^2 + \left(\frac{\chi_{a,bkg}\left(R_{532,cal} - 1\right)}{\chi_m R_{532,cal}}\right)^2 \left(\frac{\Delta \chi_{a,bkg}}{\chi_{a,bkg}}\right)^2}. \qquad (30)$$

For calculations that follow, we will assume $\Delta\chi_{a,bkg}/\chi_{a,bkg} = 0.5$ (to encompass the full range of the measurements by *Spinhirne et al.* [1997]) and $\Delta R_{532,cal}/R_{532,cal} = 0.02$ (i.e., $R_{532,cal} = 1.04 \pm 0.02$). Tabulated values of the corrected CPL color ratio are given in Table 4. Note that the ratio of two-way transmittances shown in equation 27 is assumed to be unity for this calculation. When corrected for calibration bias errors, the CPL backscatter color ratio measurements appear to confirm the earlier expectation of *Reagan et al.* [2002] that $\chi = 1$ for cirrus clouds.

[29] It is perhaps worth noting that if we assume $R_{532,cal} = 1.01$, as in the study of Tao et al., then the corrected mean value of the CPL color ratio is identical to the value derived in that work. If instead we assume $\chi_{a,bkg} = 0.375$, again as in the study of Tao et al., the CPL color ratio is 0.87 ± 0.22 for $R_{532,cal} = 1.01$ and 1.00 ± 0.25 for $R_{532,cal} = 1.04$. We also note that, given a uniform aerosol loading above and below the clouds, the bias in CPL 532 nm calibration coefficient will have essentially no effect on the magnitude of the cirrus cloud optical depths derived from direct two-way transmittance measurements (i.e., as described in section 5.3; see *Del Guasta* [1998]). For those retrievals that require an independent estimate of lidar ratio (e.g., opaque and/or subvisible layers), an overestimate of the calibration coefficient will introduce an overestimate of optical depth that is proportional to the calibration bias for small optical depths but increases nonlinearly for larger optical depths. Finally, we note that neither of the two color ratio estimation techniques discussed earlier in section 5.3 accounts for the possibility of aerosol scattering occurring simultaneously within the cirrus region. That is, a more general statement of equation (1) would expand the particulate backscatter coefficient $\beta_p(r)$ into separate contributions from clouds ($\beta_c(r)$) and aerosols ($\beta_a(r)$). Similarly, the particulate two-way transmittance would become T_p^2 (r) = T_c^2 (r) T_a^2 (r). However, given reasonable assumptions about the aerosol loading in the cirrus region (e.g., $(\beta_m(r) + \beta_a(r))/\beta_a(r) \leq 1.05$, as above), neither of these simplifications will contribute any significant perturbation to the color ratio estimates derived via equation (16) or equation (22). As explained earlier, the ratio of the aerosol two-way transmittances will be essentially equal to 1, and this holds true at cirrus altitudes as well as in the CPL calibration region. With regard to the backscatter contributions, the mean attenuated scattering ratio for the transparent cirrus clouds measured by CPL was 21.7 ± 11.1 at 532 nm and 269.5 ± 131.4 at 1064 nm. Aerosol contributions to the total backscatter can therefore be conservatively estimated at 1 part in 400 for the 532 nm channel, and (assuming = $\chi_{a,bkg} = 0.4$) 1 part in 800 at 1064 nm, suggesting a bias in the color ratios derived via the two-way transmittance measurement method of ~0.2%. The mean attenuated scattering ratios for the opaque layers were substantially higher, so that the bias for color ratios estimated using equation (22) would be concomitantly smaller.

7. Color Ratio Consistency Across Multiple Data Sets

[30] In attempting to reconcile the Tao values with the CPL and Beyerle data sets, we ask this question: for an elastic backscatter lidar operating in Hampton, Va, is 1.01 the most reasonable assumption to make for the value of $R_{532,cal}$? The analysis in the previous section would suggest that the answer is no. However, as a zenith-viewing system, the HU lidar likely calibrates much lower in the atmosphere than does the CPL, and thus, the upper troposphere/lower stratosphere values of R_{532} derived earlier from satellite-based passive sensors may not be broadly applicable to the HU calibration procedure.

[31] Accuracy in the assumed value of $R_{532,cal}$ is critically important for the calibration of elastic backscatter lidars via the molecular normalization technique. On the other hand, no such assumption is required in the analysis of HSRL and Raman measurements, as these systems can make direct measurements of R_{532}. Therefore, with some caveats, we can derive an estimate of "the most reasonable value" for $R_{532,cal}$ in the mid-to-lower troposphere using measurements acquired by the high spectral resolution lidar developed at NASA's Langley Research Center (LaRC). The LaRC HSRL is an airborne, nadir-viewing system that makes direct measurements of R_{532} for altitudes below ~8 km. Complete instrument details are given by *Hair et al.* [2008]. Measurement descriptions and instrument validation are reported by *Rogers et al.* [2009]. During the same period that Tao et al. were making their cirrus cloud measurements, the LaRC HSRL was engaged in a comprehensive CALIPSO

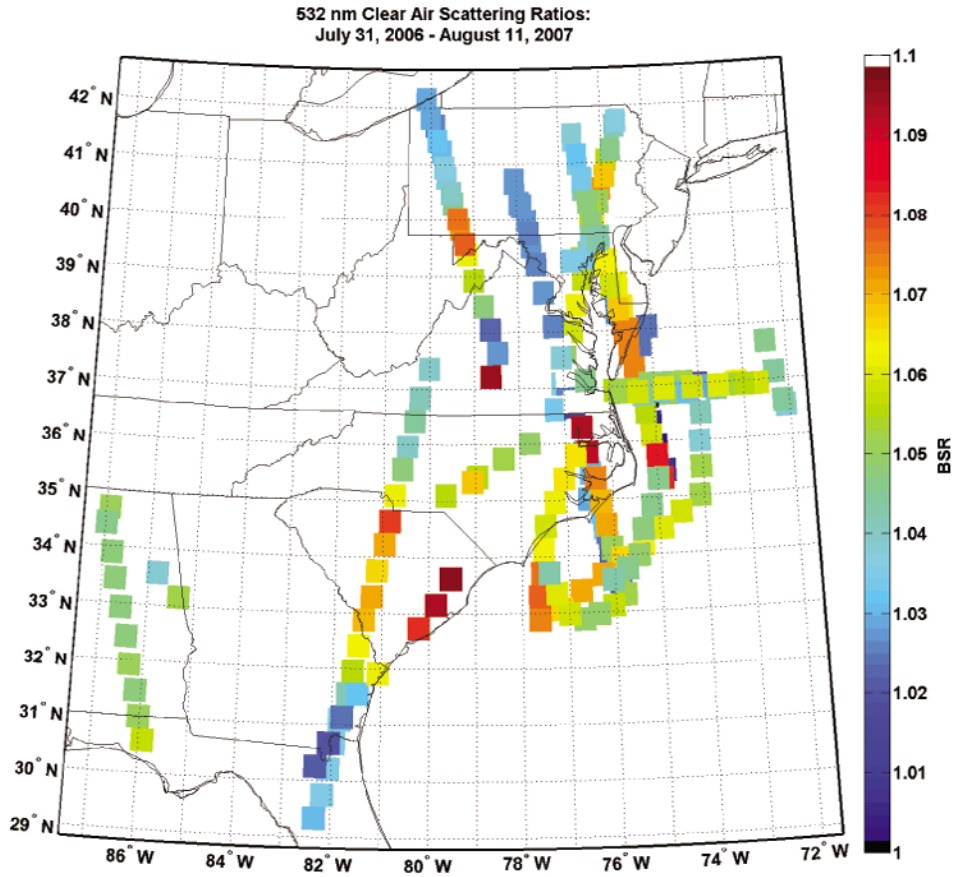

Figure 6. Locations of clear air scattering ratios measured by the LaRC airborne HSRL between 31 July 2006 and 11 August 2007. Colors indicate the scattering ratio in the clearest half-kilometer vertical extent between the instrument transmitter-receiver overlap altitude (~7.5 km) and the ground. Each measurement bin represents a horizontal distance of approximately 40 km.

validation campaign designed to assess the accuracy of the CALIOP 532 nm calibration [*Powell et al.*, 2009]. Between 31 July 31 2006 and 11 August 11 2007, the LaRC HSRL flew 24 CALIPSO validation flights that were along or near the Eastern seaboard of the United States. Flight locations are shown in Figure 6.

[32] To estimate a most reasonable value for $R_{532,\mathrm{cal}}$, we adopted the following procedure. The LaRC airborne HSRL measures aerosol scattering ratio at a spatial resolution of 30 m vertically and ~50 m horizontally. At this resolution, uncertainties in clear air regions where aerosol scattering ratios are close to 1 are estimated to be on the order of ±0.02. To reduce noise and improve the quality of the derived statistics, the 532 nm scattering ratio profiles for each flight were partitioned into a coarse grid, with each grid cell extending roughly 500 m vertically and 40 km horizontally. Each cell is then characterized using the median of the aerosol scattering ratios therein. Using the median value instead of the mean value helps eliminate contamination from thinner clouds, as cloud scattering ratios have been experimentally observed to cluster at values greater than 1.2 and thus can be easily discriminated from clear air. To eliminate contamination of the data set by dense clouds, those cells for which 50% or more of the scattering ratios exceeded 11 were excluded from subsequent analysis. Data from the first 0.5 km below the airplane were also excluded, thereby, avoiding any possible instrument transmitter-receiver overlap effects. Similarly, data acquired while the airplane was ascending or descending were excluded to ensure the scattering ratio measurements were not affected by changes in the instrument induced by changes in airplane cabin pressure and/or temperature.

[33] After constructing the grid of median values, each 40 km column within the grid is scanned vertically to determine the minimum clear air scattering ratio that would be measured by a zenith-pointing lidar. Presumably this minimum value represents the aerosol content of the "clear air" that would be used for molecular normalization by an elastic backscatter system. The frequency distribution of the clear air scattering ratios for all 24 CALIPSO validation flights is shown in Figure 7. The HSRL data indicate that the cleanest air in the lower troposphere is generally somewhat more contaminated than was assumed by Tao et al. Operating during the same time span and in the same general geographic region where the Tao measurements were made, the LaRC HSRL measured a minimum scattering ratio of 1.05 ± 0.03. This larger value is more in line with the estimates of $R_{532,\mathrm{cal}}$ derived earlier for the upper troposphere. Had they used these larger values of $R_{532,\mathrm{cal}}$, the

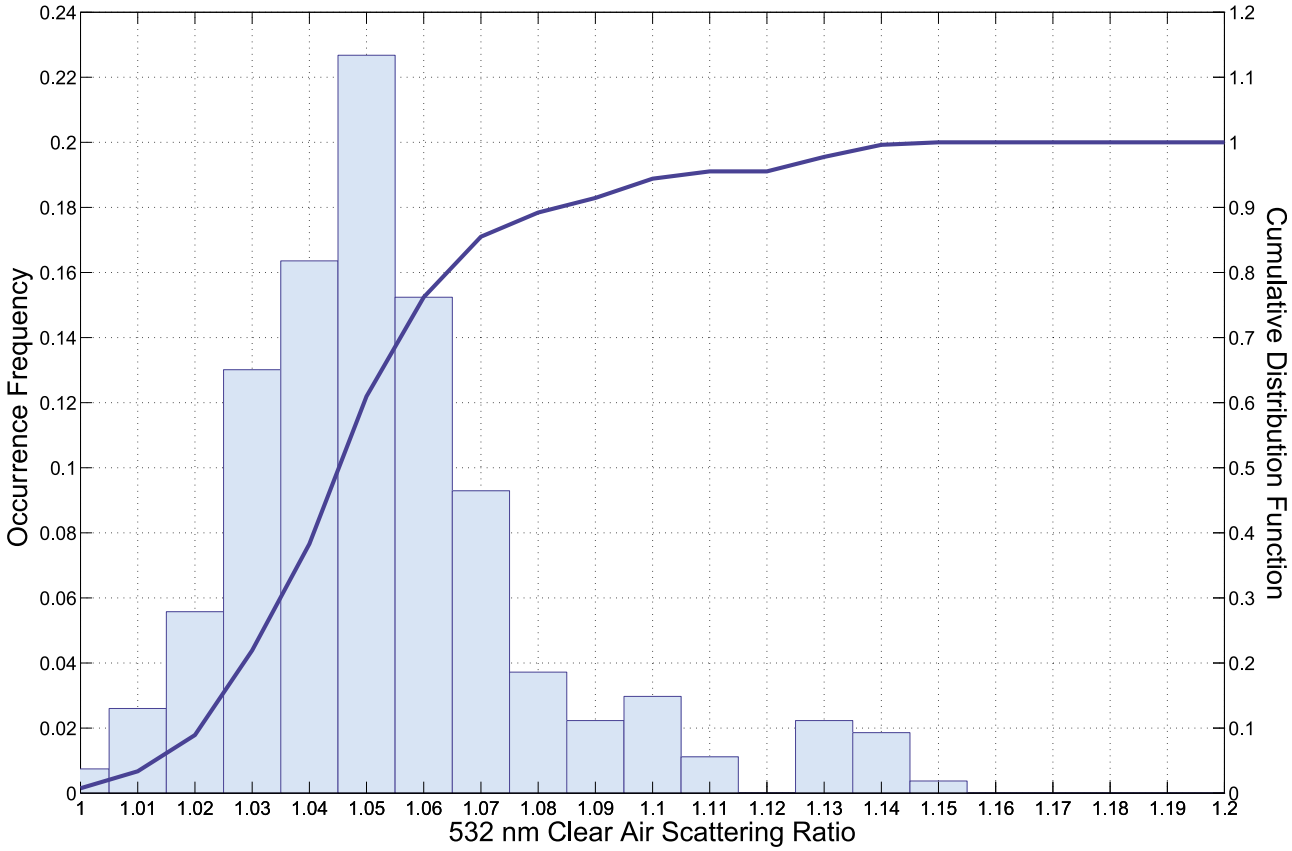

Figure 7. Occurrence frequency of scattering ratios for the clearest air measured below the LaRC airborne HSRL along the mid-Atlantic coast of the United States for 24 flights between 31 July 2006 and 11 August 2007. Profiles of 532 nm scattering ratio measurements averaged over approximately 40 km and extending from ~7.5 km to the ground were searched for the single half-kilometer bin with the lowest median scattering ratio. The 24 flights produced 269 measurements of clear air bins, all of which are plotted here.

color ratios retrieved by Tao et al. would have been closer to the value of 1 derived above for the CPL data set.

[34] The discussion above notwithstanding, it is important to note that the HSRL clear air assessment cannot be used to definitively reconcile the Tao et al. color ratio retrievals with the CPL and Beyerle results. The HSRL measurements were not coincident with the HU measurements of cirrus clouds but instead were acquired over a broader geographic region that was perhaps characterized by different background aerosol species having different values of $\chi_{a,bkg}$. There are also temporal and spatial mismatches to consider: the HSRL measurements were made predominantly during the summer months of 2006 and 2007, and the HU system had the option of calibrating well above the maximum HSRL measurement altitude of ~7.5 km.

8. Assessment of CALIPSO 1064 nm Calibration Uncertainties

[35] The statistics given in Table 4 show that the variability in backscatter color ratio for a single cirrus cloud sample is on the order of ~25%. Recent theoretical studies show a similar spread in values [*Bi et al.*, 2009]. Clearly this amount of uncertainty would be unacceptable for the CALIOP calibration algorithm, as it would introduce unmanageable error levels into several key aspects of the subsequent level II data processing. For example, the CALIOP cloud-aerosol discrimination scheme relies explicitly on color ratio [*Liu et al.*, 2009], as do some external aerosol typing methods [e.g., *McPherson and Reagan*, 2009]. However, as explained in section 3, the CALIPSO calibration routine acquires as many cirrus samples as are available during each daytime and nighttime orbit segment, and these samples are averaged together to generate the scale factor used to derive the 1064 nm calibration coefficients (see equation (10) and equation (11)). Assuming $R_{532,cal} = 1.04$ for the CPL color ratio measurements, the appropriate uncertainty estimate in color ratio used in the CALIOP calibration is $0.25/\sqrt{N}$, where N is the number of independent cirrus cloud calibration calculations made during a given orbit segment. Figure 8 shows the distribution of the number of calibration-quality cirrus cloud measurements made during all nighttime orbit segments for the CALIPSO mission to date. The mean number of cirrus observations is 185 ± 101. If we assume that these are all independent measurements, the random uncertainty in the scale factor introduced by using a color ratio estimate of 1 is on the order of 2% and thus would be a factor of 2 lower than the original, pre-launch estimates. It is clear, however, that the measurements in any one orbit segment are not necessarily

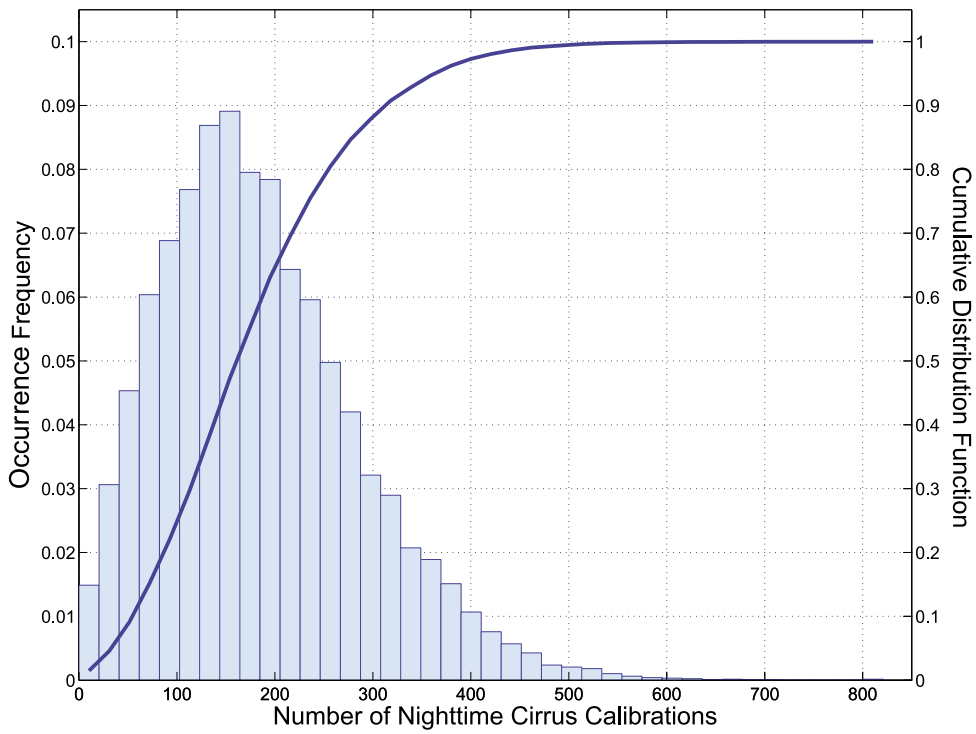

Figure 8. Frequency of dense cirrus measurements ($R' > 50$) for all CALIOP nighttime orbits from 13 June 2006 through 16 February 2009. The mean number of calibration-quality cirrus measured per orbit segment is 185 ± 101.

independent, as any one cloud can provide a number of adjacent calibration opportunities. Still, even if only 20% of the calibration measurements can be considered independent, the random uncertainty in the scale factor will still satisfy the pre-launch predictions.

[36] Perhaps the most convincing demonstration of the effectiveness of the CALIOP cirrus cloud calibration scheme would be a comparison of retrieved "clear air" backscatter coefficients to the expected values obtained from GMAO meteorological data. Making such a comparison is, however, fraught with difficulties. First, because the molecular scattering efficiency at 1064 nm is so low, bringing the molecular backscatter signal up out of the 1064 nm measurement noise requires extensive averaging of clear regions in the midtroposphere. Second, those orbits that contain sufficient stretches of uninterrupted "clear air" are

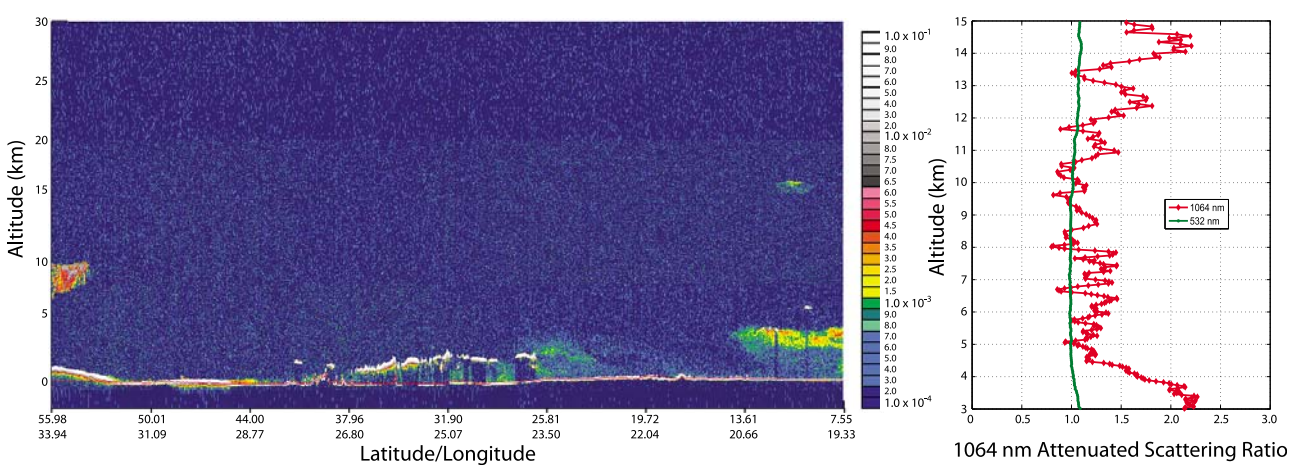

Figure 9. The left panel shows CALIOP attenuated backscatter coefficients measured at 1064 nm on 1 January 2009 over eastern Europe and north central Africa beginning at ~0022:15 UTC. The right panel shows profiles of the mean attenuated scattering ratios at both 1064 nm (in red) and 532 nm (in green). The profile data were averaged horizontally between 52°N and 14°N and smoothed vertically to 420 m resolution. Cirrus sampling in this orbit segment is quite sparse, as only 37 cirrus measurements were available for use in computing the 1064 nm calibration coefficients.

not likely to also contain a large number of calibration-quality cirrus clouds. Nevertheless, while the opportunities for such comparisons are relatively few, the necessary conditions occur often enough to illustrate the quality of the 1064 calibration. One such example is shown in Figure 9. On the first orbit segment from 1 January 2009, CALIOP measured an uninterrupted stretch of clear air extending from 52°N down to 14°N. Figure 9 (right) shows the mean attenuated backscatter coefficient profiles derived from these data at both 532 and 1064 nm. As expected, SNR of the 1064 nm profile is substantially lower than that of the 532 nm profile. Despite the additional noise, the 1064 nm attenuated scattering ratios are seen to hover about a mean value of 1 in the cleanest portion of the atmosphere, with a mean value of 1.00 ± 0.39 between 8 and 10.5 km.

9. Closing Remarks

[37] Accurate calibration of the 1064 nm channel for space-based lidars is a daunting and demanding task. To date, all space lidar missions have chosen to use cirrus clouds as their primary calibration target. Successful use of use cirrus clouds as a calibration target requires that the characteristic backscatter color ratio of cirrus and its associated natural variability both be well known. The assumption made at the beginning of the CALIPSO mission was that strongly scattering cirrus ($R' > 50$) were well characterized by a value of $\chi_{\mathrm{cirrus}} = 1.00 \pm 0.04$. In this work we have used over 400 h of measurements acquired by the Cloud Physics Lidar to demonstrate that, in general, this pre-launch assumption remains valid and that the mean backscatter color ratio of cirrus clouds is approximately 1. However, the measured variability of cirrus color ratios is much larger than previously realized, roughly ±25%, versus the pre-launch estimate of ±4% given by *Reagan et al.* [2002]. The CPL measurements reinforce the observation first made by *Beyerle et al.* [2001] that the color ratio distribution for cirrus clouds is much broader than might be expected solely from geometric optics considerations. Calibration using measurements from a single cloud is, therefore, ill advised, as doing so may lead to significant errors. To obtain a reliable calibration from cirrus, a large number of clouds should be sampled. Because the CALIOP 1064 nm calibration scheme computes estimates of the 1064 calibration coefficients using a scale factor derived from the average of all cirrus clouds detected within an orbit segment, sampling errors that might otherwise skew the calibration estimates are minimized. Thus, the main conclusions we draw from this study are somewhat anticlimactic but nonetheless gratifying. First, we find that the best estimate for the backscatter color ratio of cirrus clouds is $\chi_{\mathrm{cirrus}} = 1.01 \pm 0.25$, thus, confirming the assumptions and measurements presented in previous studies. Second, as a consequence of the first finding, we are reassured that the CALIOP 1064 nm calibration algorithm uses the appropriate value for the cirrus backscatter color ratio ($\chi_{\mathrm{cirrus}} = 1$), and the pre-launch estimates of ~10% for the calibration uncertainty remain achievable.

[38] The intent of this study was not to examine individual measurements and then offer learned explanations for the observed variabilities. No doubt there is much that could be learned from such an exercise. (One example, why are the measured color ratios so much higher in the tropics? Was the tropopause region especially clean during the TC4 campaign, so that $R_{532,\mathrm{cal}} = 1$ was indeed the appropriate assumption?) However, the CALIOP 1064 nm calibration scheme that motivated this analysis relies on and thus requires an accurate assessment of the global mean value of χ_{cirrus}. It seems quite fortuitous then that, after applying a number of independently derived assessments of mean aerosol properties and loading, the cirrus cloud color ratio measured by CPL still comes out so close to the historically expected value of 1. While the mean aerosol loading in the CPL calibration region is well documented (e.g., in the SPARC report), global mean values of the aerosol intrinsic properties (S_{532} and χ_a) required to convert the extinction data measured by passive satellites into the backscatter estimates required by lidars are much more uncertain. As more information becomes available on the intensive properties of the background aerosol in the CPL calibration region (nominally 12 to 15 km), our current evaluation of χ_{cirrus} will need to be revisited.

[39] **Acknowledgments.** We gratefully acknowledge NASA-HQ program manager Hal Maring for his continued support of the Multi-Instrument Data Analysis and Synthesis (MIDAS) project. Our heartfelt thanks go also to John Reagan for useful discussions on the backscatter color ratio for background aerosols, to Larry Thomason and Chip Trepte for insights into the magnitudes and uncertainties of stratospheric aerosol extinction coefficients, to Chris Hostetler and John Hair for their tutelage on HSRL measurements of "clear air," to Ralph Kuehn for numerous and fruitful conversations about the intricacies of lidar data acquisition and analysis, and to Dave Winker for insightful comments that helped to improve the manuscript.

References

Althausen, D., D. Müller, A. Ansmann, U. Wandinger, H. Hube, E. Clauder, and S. Zörner (2000), Scanning 6-Wavelength 11-Channel Aerosol Lidar, *J. Atmos. Oceanic Technol.*, *17*, 1469–1482.

Ansmann, A., U. Wandinger, M. Riebesell, C. Weitkamp, and W Michaelis. (1992), Independent measurement of extinction and backscatter profiles in cirrus-clouds by using a combined Raman elastic-backscatter lidar, *Appl. Opt.*, *31*, 7113–7131.

Ansmann, A., et al. (1993), Lidar network observations of cirrus morphological and scattering properties during the International Cirrus Experiment 1989: The 18 October 1989 case study and statistical analysis, *J. Appl. Meteorol.*, *32*, 1608–1622.

Atlas, D., Z. Wang, and D. P. Duda (2006), Contrails to cirrus—morphology, microphysics, and radiative properties, *J. Clim. Appl. Meteorol.*, *45*, 5–19.

Balis, D., et al. (2006), Optical characteristics of desert dust over the East Mediterranean during summer: a case study, *Ann. Geophys.*, *24*, 807–821.

Bevington, P. R., and D. K. Robinson (1992), *Data Reduction and Error Analysis for the Physical Sciences*, 328 pp., McGraw-Hill, New York.

Beyerle, G., M. R. Gross, D. A. Haner, N. T. Kjome, I. S. McDermid, T. J. McGee, J. M. Rosen, H.-J. Schäfer, and O. Schrems (2001), A lidar and backscatter sonde measurement campaign at Table Mountain during February–March 1997: Observations of cirrus clouds, *J. Atmos. Sci.*, *58*, 1275–1287.

Bi, L., P. Yang, G. Kattawar, B. A. Baum, Y. X. Hu, D. M. Winker, R. S. Brock, and J. Q. Lu (2009), Simulation of the color ratio associated with the backscattering of radiation by ice crystals at 0.532- and 1.064-μm wavelengths, *J. Geophys. Res.*, *114*, D00H08, doi:10.1029/2009JD011759.

Bloom, S., et al. (2005), Documentation and validation of the Goddard Earth Observing System (GEOS) Data Assimilation System, version 4. Technical Report Series on Global Modeling and Data Assimilation, NASA/TM-2005-104606, 26, 165 pp. (Available online at http://gmao.gsfc.nasa.gov/pubs/tm/)

Bohren, C. F., and D. R. Huffman (1983), *Absorption and Scattering of Light by Small Particles*, 530 pp., John Wiley, New York.

Bodhaine, B. A., N. B. Wood, E. G. Dutton, and J. R. Slusser (1999), On Rayleigh Optical Depth Calculations, *J. Atmos. Oceanic Technol.*, *16*, 1854–1861.

Bucholtz, A. (1995), Rayleigh-scattering calculations for the terrestrial atmosphere, *Appl. Opt.*, *34*, 2765–2773.

Cattrall, C., J. Reagan, K. Thome, and O. Dubovik (2005), Variability of aerosol and spectral lidar and backscatter and extinction ratios of key aerosol types derived from selected Aerosol Robotic Network locations, *J. Geophys. Res.*, *110*, D10S11, doi:10.1029/2004JD005124.

Chen, W. N., C. C. Tsao, and J. B. Nee (2004), Rayleigh lidar temperature measurements in the upper troposphere and lower stratosphere, *J. Atmos. Sol-Terr. Phy.*, *66*, 39–49.

Chen, W.-N., F.-J. Tsai, C. C.-K. Chou, S.-Y. Chang, Y.-W. Chen, and J.-P. Chen (2007), Optical properties of Asian dusts in the free atmosphere measured by Raman lidar at Taipei, Taiwan, *Atmos. Environ.*, *41*, 7698–7714, doi:10.1016/j.atmosenv.2007.06.001.

Del Guasta, M. (1998), Errors in the retrieval of thin-cloud optical parameters obtained with a two-boundary algorithm, *Appl. Opt.*, *37*, 5522–5540.

Del Guasta, M., and K. Niranjan (2001), Observation of Low-Depolarization Contrails at Florence (Italy) using a 532–1064 nm Polarization LIDAR, *Geophys. Res. Lett.*, *28*(21), 4067–4070.

DeSlover, D. H., et al. (2007), High spectral resolution infrared closure study applied to TC4 cloud property retrievals, *Eos Trans. AGU*, *88*(52), Fall Meet. Suppl., Abstract A13C-1366.

Fernald, F. G. (1984), Analysis of atmospheric lidar observations: some comments, *Appl. Opt.*, *23*, 652–653.

Gobbi, G. P. (1995), Lidar estimation of stratospheric aerosol properties: Surface, volume, and extinction to backscatter ratio, *J. Geophys. Res.*, *100*(D6), 11219–11235.

Gobbi, G. P. (1998), Parameterization of stratospheric aerosol physical properties on the basis of Nd:YAG lidar observations, *Appl. Opt.*, *37*, 4712–4720.

Grund, C. J., and E. W. Eloranta (1990), The 27–28 October 1986 FIRE IFO cirrus case study: Cloud optical properties determined by high spectral resolution lidar, *Mon. Weather Rev.*, *118*, 2344–2355.

Hair, J., C. Hostetler, A. Cook, D. Harper, R. Ferrare, T. Mack, W. Welch, L. Izquierdo, and F. Hovis (2008), Airborne high spectral resolution lidar for profiling aerosol optical properties, *Appl. Opt.*, *47*, 6734–6752.

Hart, W. D., J. D. Spinhirne, S. P. Palm, and D. L. Hlavka (2005), Height distribution between cloud and aerosol layers from the GLAS spaceborne lidar in the Indian Ocean region, *Geophys. Res. Lett.*, *32*, L22S06, doi:10.1029/2005GL023671.

Hlavka, D. L., S. P. Palm, W. D. Hart, J. D. Spinhirne, M. J. McGill, and E. J. Welton (2005), Aerosol and cloud optical depth from GLAS: Results and verification for an October 2003 California fire smoke case, *Geophys. Res. Lett.*, *32*, L22S07, doi:10.1029/2005GL023413.

Hostetler, C. A., Z. Liu, J. A. Reagan, M. A. Vaughan, D. M. Winker, M. T. Osborn, W. H. Hunt, K. A. Powell, and C. R. Trepte (2005), CALIPSO algorithm theoretical basis document, PC-SCI-201. (Available online at http://www-calipso.larc.nasa.gov/resources/project_documentation.php)

Hu, Y., Z. Liu, D. Winker, M. Vaughan, V. Noel, L. Bissonnette, G. Roy, and M. McGill (2006), A simple relation between lidar multiple scattering and depolarization for water clouds, *Opt. Lett.*, *31*, 1809–1811.

Hu, Y, M. Vaughan, Z. Liu, K. Powell, and S. Rodier (2007), Retrieving optical depths and lidar ratios for transparent layers above opaque water clouds from CALIPSO lidar measurements, *IEEE Geosci. Remote Sens. Lett.*, *4*, 523–526.

Hunt, W. H., D. M. Winker, M. A. Vaughan, K. A. Powell, P. L. Lucker, and C. Weimer (2009), CALIPSO lidar description and performance assessment, *J. Atmos. Oceanic Technol.*, *26*, 1214–1228, doi:10.1175/2009JTECHA1223.1.

Immler, F., and O. Schrems (2003), Vertical profiles, optical and microphysical properties of Saharan dust layers determined by a ship-borne lidar, *Atmos. Chem. Phys.*, *3*, 1353–1364.

Immler, F., K. Krüger, S. Tegtmeier, M. Fujiwara, P. Fortuin, G. Verver, and O. Schrems (2007), Cirrus clouds, humidity, and dehydration in the tropical tropopause layer observed at Paramaribo, Suriname (5.8°N, 55.2°W), *J. Geophys. Res.*, *112*, D03209, doi:10.1029/2006JD007440.

Liu, Z., M. A. Vaughan, D. M. Winker, C. Kittaka, R. E. Kuehn, B. J. Getzewich, C. R. Trepte, and C. A. Hostetler (2009), The CALIPSO lidar cloud and aerosol discrimination: Version 2 algorithm and initial assessment of performance, *J. Atmos. Oceanic Technol.*, *26*, 1198–1213, doi:10.1175/2009JTECHA1229.1.

Kent, G. S., P.-H. Wang, and K. M. Skeens (1997), Discrimination of cloud and aerosol in the Stratospheric Aerosol and Gas Experiment III occultation data, *Appl. Opt.*, *36*, 8639–8649.

Mattis, I., A. Ansmann, U. Wandinger, and D. Müller (2003), Unexpectedly high aerosol load in the free troposphere over central Europe in spring/summer 2003, *Geophys. Res. Lett.*, *30*(22), 2178, doi:10.1029/2003GL018442.

Mattis, I., A. Ansmann, D. Müller, U. Wandinger, and D. Althausen (2004), Multiyear aerosol observations with dual wavelength Raman lidar in the framework of EARLINET, *J. Geophys. Res.*, *109*, D13203, doi:10.1029/2004JD004600.

McGill, M. J., D. L. Hlavka, W. D. Hart, J. D. Spinhirne, V. S. Scott, and B. Schmid (2002), The Cloud Physics Lidar: Instrument description and initial measurement results, *Appl. Opt.*, *41*, 3725–3734.

McGill, M. J., D. L. Hlavka, W. D. Hart, E. J. Welton, and J. R. Campbell (2003), Airborne lidar measurements of aerosol optical properties during SAFARI-2000, *J. Geophys. Res.*, *108*(D13), 8493, doi:10.1029/2002JD002370.

McGill, M. J., L. Li, W. D. Hart, G. M. Heymsfield, D. L. Hlavka, P. E. Racette, L. Tian, M. A. Vaughan, and D. M. Winker (2004), Combined lidar-radar remote sensing: Initial results from CRYSTAL-FACE, *J. Geophys. Res.*, *109*(D7), D07203, doi: 10.1029/2003JD004030.

McGill, M. J., M. A. Vaughan, C. R. Trepte, W. D. Hart, D. L. Hlavka, D. M. Winker, and R. Kuehn (2007), Airborne validation of spatial properties measured by the CALIPSO lidar, *J. Geophys. Res.*, *112*, D20201, doi:10.1029/2007JD008768.

McPherson, C., and J. Reagan (2009), Analysis of optical properties of Saharan dust derived from dual-wavelength aerosol retrievals from CALIPSO observations, *IEEE Geosci. Remote Sens. Lett.*, in press.

Menzies, R. T., D. M. Tratt, and W. H. Hunt (1998), Lidar In-space Technology Experiment measurements of sea surface directional reflectance and the link to surface wind speed, *Appl. Opt.*, *37*, 5550–5559.

Noel, V., D. M. Winker, M. McGill, and P. Lawson (2004), Classification of particle shapes from lidar depolarization ratio in convective ice clouds compared to in situ observations during CRYSTAL-FACE, *J. Geophys. Res.*, *109*, D24213, doi:10.1029/2004JD004883.

Miller, M. A. (2008), The Cloud and Land Surface Interaction Campaign (CLASIC), *Eos Trans. AGU*, *89*(23), Jt. Assem. Suppl., Abstract H43D-03.

O'Connor, E. J., A. J. Illingworth, and R. J. Hogan (2004), A Technique For Autocalibration Of Cloud Lidar, *J. Atmos. Ocean. Technol.*, *21*, 777–786.

Omar, A., et al. (2009), The CALIPSO automated aerosol classification and lidar ratio selection algorithm, *J. Atmos. Oceanic Technol.*, *26*, 1994–2014, doi:10.1175/2009JTECHA1231.1.

Osborn, M. T. (1998), Calibration of LITE data, in *Proceedings of the 19th International Laser Radar Conference*, NASA/CP-19980227633, 245–247.

Palm, S. P., W. D. Hart, D. L. Hlavka, E. J. Welton, A. Mahesh, and J. D. Spinhirne (2002), Geoscience Laser Altimeter System (GLAS) algorithm theoretical basis document version 4.2; Atmospheric Data Products. (Available online at http://eospso.gsfc.nasa.gov/eos_homepage/for_scientists/atbd/viewInstrument.php?instrument=6)

Palm, S., D. Hlavka, W. Hart, J. Spinhirne, and M. McGill (2004), Calibration of the Geoscience Laser Altimeter System (GLAS) atmospheric channels, in *Proceedings of the 22nd International Laser Radar Conference*, ESA SP-561, 1003–1006.

Platt, C. M. R. (1973), Lidar and radiometric observations of cirrus clouds, *J. Atmos. Sci.*, *30*, 1191–1204.

Powell, K. A., M. A. Vaughan, R. Kuehn, W. H. Hunt, and K.-P. Lee (2008), Revised calibration strategy for the CALIOP 532 nm channel: Part II, Daytime, reviewed and revised papers presented at the 24th International Laser Radar Conference, ISBN 978-0-615-21489-4, 1177–1180.

Powell, K. A., C. A. Hostetler, Z. Liu, M. A. Vaughan, R. E. Kuehn, W. H. Hunt, K. Lee, C. R. Trepte, and D. M. Winker (2009), CALIPSO lidar calibration algorithms: Part I, Nighttime 532 nm parallel channel and 532 nm perpendicular channel, *J. Atmos. Oceanic Technol.*, *26*, 2015–2033, doi:10.1175/2009JTECHA1242.1.

Ramachandran, S., and A. Jayaraman (2003), Balloon-borne study of the upper tropospheric and stratospheric aerosols over a tropical station in India, *Tellus B*, *55*, 820–836.

Reagan, J. A., and D. A. Zielinskie (1991), Spaceborne lidar remote sensing techniques aided by surface returns, *Opt. Eng.*, *30*, 96–102.

Reagan, J. A., X. Wang, and M. T. Osborn (2002), Spaceborne lidar calibration from cirrus and molecular backscatter returns, *IEEE Trans. Geosci. Remote Sens.*, *40*, 2285–2290.

Rogers, R. R., et al. (2009), NASA LaRC airborne high spectral resolution lidar aerosol measurements during MILAGRO: observations and validation, *Atmos. Chem. Phys.*, *9*, 4811–4826.

Russell, P. B., T. J. Swissler, and M. P. McCormick (1979), Methodology for error analysis and simulation of lidar aerosol measurements, *Appl. Opt.*, *18*, 3783–3797.

Sassen, K., and S. Benson (2001), A midlatitude cirrus cloud climatology from the Facility for Atmospheric Remote Sensing. Part II: Microphysical properties derived from lidar depolarization, *J. Atmos. Sci.*, *58*, 2103–2112.

Schneider, J., and R. Eixmann (2002), Three years of routine Raman lidar measurements of tropospheric aerosols: Backscattering, extinction, and residual layer height, *Atmos. Chem. Phys.*, *2*, 313–323.

Spinhirne, J. D., S. Chudamani, J. F. Cavanaugh, and J. L. Bufton (1997), Aerosol and cloud backscatter at 1.06, 1.54, and 0.53 mm by airborne hard-target-calibrated Nd:YAG/methane Raman lidar, *Appl. Opt.*, *36*, 3475–3490.

Spinhirne, J. D., S. P. Palm, W. D. Hart, D. L. Hlavka, and E. J. Welton (2005), Cloud and aerosol measurements from GLAS: Overview and initial results, *Geophys. Res. Lett.*, *32*, L22S03, doi:10.1029/2005GL023507.

Su, W., G. L. Schuster, N. G. Loeb, R. R. Rogers, R. A. Ferrare, C. A. Hostetler, J. W. Hair, and M. D. Obland (2008), Aerosol and cloud interaction observed from high spectral resolution lidar data, *J. Geophys. Res.*, *113*, D24202, doi:10.1029/2008JD010588.

Sugimoto, N., I. Matsui, Z. Liu, A. Shimizu, K. Asai, K. Yoneyama and M. Katsumata (2001), Latitudinal distribution of aerosols and clouds in the western Pacific observed with a lidar on board the research vessel Mirai, *Geophys. Res. Lett.*, *28*(22), 4187–4190, doi:10.1029/2001GL013510.

Tao, Z., M. P. McCormick, D. Wu, Z. Liu, and M. A. Vaughan (2008), Measurements of cirrus cloud backscatter color ratio with a two-wavelength lidar, *Appl. Opt.*, *47*, 1478–1485.

Thomason, L., and T. Peter (2006), Assessment of Stratospheric Aerosol Properties (ASAP), SPARC Report No.4, WCRP-124, WMO/TD-No. 1295. (Available online at http://www.atmosp.physics.utoronto.ca/SPARC/PublicationIndex.html)

Vanhellemont, F., et al. (2008), Aerosol extinction profiles at 525 nm and 1020 nm derived from ACE imager data: comparisons with GOMOS, SAGE II, SAGE III, POAM III, and OSIRIS, *Atmos. Chem. Phys.*, *8*, 2027–2037.

Vaughan, M. A., D. M. Winker, and K. A. Powell (2005), CALIOP Algorithm theoretical basis document, Part 2: Feature detection and layer properties algorithms, PC-SCI-202.01, NASA Langley Research Center, Hampton, Va 23681, 87 pp. (Available online at http://www-calipso.larc.nasa.gov/resources/project_documentation.php)

Winker, D. M., R. Couch, and M. P. McCormick (1996), An overview of LITE: NASA's Lidar In-space Technology Experiment, *Proc. IEEE*, *84*, 164–180.

Winker, D. (2003), Accounting for multiple scattering in retrievals from space lidar, *Proc. SPIE*, *5059*, 128–139.

Winker, D. M., M. A. Vaughan, A. H. Omar, Y. Hu, K. A. Powell, Z. Liu, W. H. Hunt, and S. A. Young (2009), Overview of the CALIPSO mission and CALIOP data processing algorithms, *J. Atmos. Oceanic Technol.*, *26*, 2310–2323, doi:10.1175/2009JTECHA1281.1.

Young, S. A. (1995), Analysis of lidar backscatter profiles in optically thin clouds, *Appl. Opt.*, *34*, 7019–7031.

Zhou, D. K., W. L. Smith Sr., X. Liu, A. M. Larar, H.-L. A. Huang, J. Li, M. J. McGill, and S. A. Mango (2005), Thermodynamic and cloud parameter retrieval using infrared spectral data, *Geophys. Res. Lett.*, *32*, L15805, doi:10.1029/2005GL023211.

Y. Hu, M. D. Obland, and M. A. Vaughan, Climate Science Branch, NASA Langley Research Center, 100 NASA Rd., Hampton, VA 23681, USA. (mark.a.vaughan@nasa.gov)

Z. Liu, National Institute of Aerospace, NASA Langley Research Center, 100 Exploration Way, Hampton, VA 23666, USA.

M. J. McGill, Mesoscale Atmospheric Processes Branch, NASA Goddard Space Flight Center, Code 613.1, Bldg. 33, Room A410, Greenbelt, MD 20771, USA.